}essentials{

Rudolf P. Huebener

History and Theory of Superconductors

A Compact Introduction

Springer

essentials

Springer essentials

Springer essentials provide up-to-date knowledge in a concentrated form. They aim to deliver the essence of what counts as "state-of-the-art" in the current academic discussion or in practice. With their quick, uncomplicated and comprehensible information, essentials provide:

- an introduction to a current issue within your field of expertis
- an introduction to a new topic of interest
- an insight, in order to be able to join in the discussion on a particular topic

Available in electronic and printed format, the books present expert knowledge from Springer specialist authors in a compact form. They are particularly suitable for use as eBooks on tablet PCs, eBook readers and smartphones. *Springer essentials* form modules of knowledge from the areas economics, social sciences and humanities, technology and natural sciences, as well as from medicine, psychology and health professions, written by renowned Springer-authors across many disciplines.

More information about this subseries at http://www.springer.com/series/16761

Rudolf P. Huebener

History and Theory of Superconductors

A Compact Introduction

Springer

Rudolf P. Huebener
Universität Tübingen
Tübingen, Germany

ISSN 2197-6708 ISSN 2197-6716 (electronic)
essentials
ISSN 2731-3107 ISSN 2731-3115 (electronic)
Springer essentials
ISBN 978-3-658-32379-0 ISBN 978-3-658-32380-6 (eBook)
https://doi.org/10.1007/978-3-658-32380-6

Responsible Editor: Lisa Edelhaeuser
This Springer imprint is published by the registered company Springer Fachmedien Wiesbaden GmbH part of Springer Nature.
The registered company address is: Abraham-Lincoln-Str. 46, 65189 Wiesbaden, Germany

What You Can Find in This *essential*

- An overview over more than 100 years of superconductivity
- The development of the theory of superconductors from Albert Einstein to Bardeen, Cooper, and Schrieffer
- The origin of the Josephson electronics
- The impact of moving magnetic flux quanta
- The applications of superconductors in microelectronics and in power electronics

For Christoph

Acknowledgment

The author would like to thank Benedikt Ferdinand and Matthias Rudolph for computer support and Silvia Haindl for literature references to Chaps. 10 and 11.

Contents

1 The Discovery: Kamerlingh Onnes in Leiden

In the last years of the nineteenth century, Heike Kamerlingh Onnes set up a laboratory for low-temperature experiments in Leiden, which soon became the world leader in this field. Kamerlingh Onnes was interested in the thermodynamic properties of gases and liquids at low temperatures. He was inspired by the research work of Johannes Diderik van der Waals at the University of Amsterdam. He had published his Law of Corresponding States in 1880.

At that time, competition between several laboratories in Europe had broken out in the generation of low temperatures and the associated liquefaction of gases. An important impetus for the large-scale liquefaction of gases was the announcement in 1895 of the application of the Joule–Thomson effect by Carl von Linde in Germany and William Hampson in England. The Joule–Thomson effect causes a slight reduction in the temperature of gases during isenthalpic expansion. In the same year, von Linde was able to produce liquid air for the first time by combining the Joule–Thomson effect with the countercurrent heat exchanger already proposed by Werner Siemens in 1857. In this Linde process, the highly compressed air in the heat exchanger is additionally cooled by the returning gas until its condensation temperature is reached. This process also forms the basic principle for the liquefaction of neon, hydrogen and, most recently, helium in an effort to achieve even lower temperatures.

On July 9/10, 1908, the team of Kamerlingh Onnes succeeded for the first time in liquefying helium as the last remaining noble gas, thus achieving the then record value of 4 K (−269 °C) at low temperatures. In 1911, Kamerlingh Onnes then made an astonishing discovery during cooling: below a certain temperature, the electrical resistance of certain metals disappears completely and can no longer be detected experimentally. This was the first time the phenomenon of "superconductivity," as it was subsequently called, had been observed. On April

R. P. Huebener, *History and Theory of Superconductors,* Springer essentials,
https://doi.org/10.1007/978-3-658-32380-6_1

28, 1911, Kamerlingh Onnes reported on this for the first time to the Academy in Amsterdam.

After Kamerlingh Onnes had opened up a much lower temperature range than had been possible until then, he became interested, among other things, in the question of how the electrical resistance of metals behaves at these low temperatures. At that time, there were three predictions about how the resistance changes at low temperatures as the temperature decreases: (1) the resistance decreases and reaches zero, (2) it remains constant, and (3) it increases again. Mercury appeared to be particularly suitable for accurate measurements because its low melting point makes it relatively easy to produce with a high degree of purity. The measurements should be disturbed by impurities as little as possible. Therefore, a thin glass capillary filled with mercury was used for the measurements. On April 8, 1911, Heike Kamerlingh Onnes and his team observed how the electrical resistance of the sample decreased with decreasing temperature. However, when the temperature finally reached 4 K, the curve showed a sharp bend, and the resistance dropped to an unmeasurably small value (Fig. 1.1).

After superconductivity was discovered in mercury, it was also found in other metals, alloys and metallic compounds. Among the first superconducting metals found, besides mercury, are: aluminum, lead, indium, zinc and tin.

When Kamerlingh Onnes soon began to investigate the question of whether superconductivity could be used technically for the energy industry even at high electric currents, he had to discover that the magnetic field generated by the currents was very harmful to superconductivity. In addition to the critical temperature T_C, which must not be exceeded, there is also a critical magnetic field H_C, above which superconductivity disappears. The temperature dependence of the critical magnetic field $H_C(T)$ is shown in Fig. 1.2: From the value zero at $T = T_C$, the critical magnetic field increases with decreasing temperature and reaches its maximum value at $T = 0$.

The so-called *intrinsic magnetic field* of an electric current has the same effect as a magnetic field generated by an external magnetic coil. In the literature, this connection is called *Silsbee's rule*. Thus, in addition to the critical quantities T_C and H_C, there is also a critical electric current density I_C, which must not be exceeded if superconductivity is to be maintained.

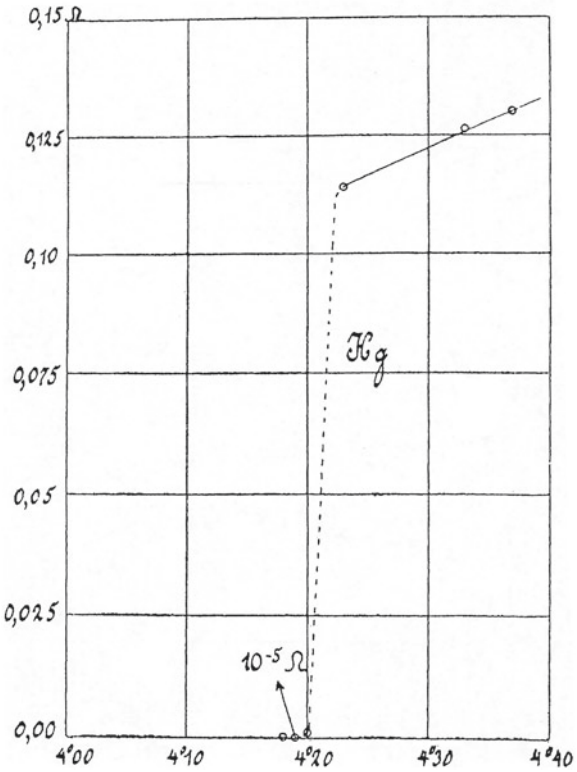

Fig. 1.1 Discovery of superconductivity. Electrical resistance in ohms of a mercury sample plotted against temperature in Kelvin. (H. Kamerlingh Onnes)

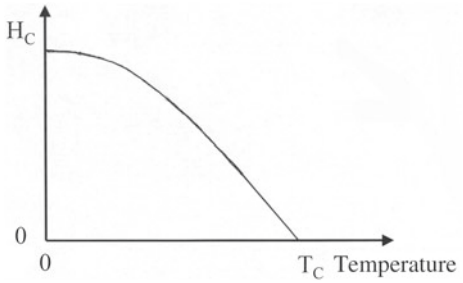

Fig. 1.2 Temperature dependence of the critical magnetic field H_C. (schematic)

2 Walther Meissner and the Physikalisch-Technische Reichsanstalt in Berlin

The Physikalisch-Technische Reichsanstalt in Berlin was also interested in material properties at low temperatures at the time. In 1913 Walther Meissner was commissioned by Emil Warburg, the president of the Reichsanstalt, to build a hydrogen liquefaction plant. Before studying physics, Meissner had already graduated as a mechanical engineer, so he was well prepared for this task. At the beginning of 1913, he was able to commission an improved liquefier based on a design by Walther Nernst. At that time, Meissner was mainly concerned with electrical resistance measurements at low temperatures.

The outbreak of the First World War in 1914 led to a significant interruption of basic physics research in many countries, including the Berlin Reichsanstalt. Subsequently, in the years 1918–1922, Meissner was particularly concerned with the enlargement of the hydrogen liquefaction plant and, from 1920 onward, increasingly with the possibility of setting up a plant for the liquefaction of helium. His plans and drafts could be realized in the years 1922–1924. On March 7, 1925, helium was liquefied for the first time in the Reichsanstalt. In the process, about 200 cm^3 of liquid helium was obtained. The Reichsanstalt was the third place in the world where experiments with liquid helium could be carried out, after Leiden as the first and from 1923 Toronto in Canada as the second place. As members of the Reichsanstalt's board of trustees, Carl von Linde and Wilhelm Conrad Röntgen had at the time strongly advocated the establishment of a cryogenic laboratory.

It is said that Walther Meissner carried out his measurements with only 0.3 L of liquid helium for 10 years. Before he appeared, five superconducting elements were known: Lead, mercury, tin, thallium and indium. In 1928, Meissner discovered another superconducting element: tantalum with a critical temperature of 4.4 K. During the following 2 years, he discovered superconductivity in thorium, titanium and niobium as well as in a number of compounds and alloys.

R. P. Huebener, *History and Theory of Superconductors,* Springer essentials,
https://doi.org/10.1007/978-3-658-32380-6_2

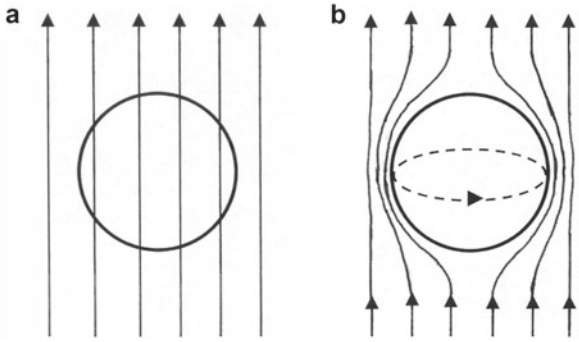

Fig. 2.1 Meissner-Ochsenfeld effect. **a** In the normal state above its critical temperature, the spherical superconductor is permeated by the external magnetic field. **b** Below the critical temperature, the superconductor expells the magnetic field completely from its interior as long as the critical magnetic field is not exceeded. The field expulsion is caused by electric currents that flow around the surface of the superconductor without loss and shield the interior of the superconductor from the magnetic field

During his term of office from 1922 to 1924 as president of the Reichsanstalt, Walther Nernst, who was known for his farsightedness, had realized that the experimental physicists of the Reichsanstalt could well use the support of a theorist. Nernst was able to enlist the help of Max von Laue, who took up his post as theoretical physicist at the Reichsanstalt on March 24, 1925 (one day a week in addition to his teaching activities at the University of Berlin). At that time, von Laue was interested in superconductivity and especially in its magnetic properties. He maintained close contact with Walther Meissner and in 1933 persuaded him to take precise measurements of an applied magnetic field near the surface of a superconductor at the transition from normal conduction to superconductivity. Von Laue was also able to help finance an additional employee for these experiments from a support program for unemployed young scientists at the time.

This is how Walther Meissner and his colleague Robert Ochsenfeld made a highly momentous discovery in 1933: In the superconducting state, a magnetic field inside the superconductor disappears by being forced out of it. Since then, this phenomenon has been known as the Meissner-Ochsenfeld effect (often abbreviated to Meissner effect) (Fig. 2.1). Thus, a superconductor (below the critical magnetic field $H_C(T)$) behaves like a perfect diamagnet.

The existence of the Meissner-Ochsenfeld effect allows an important conclusion: The superconducting state is a thermodynamic equilibrium state. Thus, the

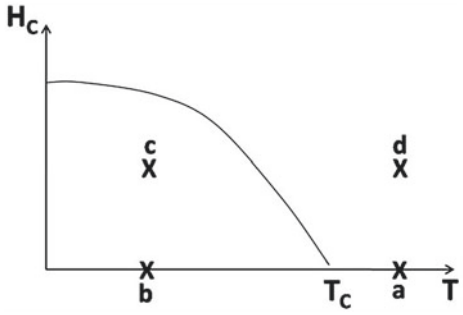

Fig. 2.2 Independence of the superconducting state from the path. Due to the Meissner-Ochsenfeld effect, the final state $B = 0$ is reached at point c on the two paths $a \rightarrow d \rightarrow c$ and $a \rightarrow b \rightarrow c$

state is independent of the path that led to it. If the magnetic field and/or the temperature changes, in the end only the following must apply: $T < T_C$ and $H < H_C(T)$.

Cornelis Jacobus Gorter and Hendrik Brugt Gerhard Casimir were the first to recognize this fundamental importance of the Meissner-Ochsenfeld effect in 1934. Their conclusion is explained in Fig. 2.2. The point c marks the superconducting state below the critical temperature T_C and the critical magnetic field $H_C(T)$. Infinite electrical conductivity without existence of the Meissner-Ochsenfeld effect on the path $a \rightarrow b \rightarrow c$ would result in the state with $B = 0$, while the path $a \rightarrow d \rightarrow c$ would result in the state with $B \neq 0$ of point d. Only the existence of the Meissner-Ochsenfeld effect ensures that the state with $B = 0$ (perfect diamagnetism) is always reached (independent of the path covered). However, it is assumed that the superconductor shows perfect reversibility and that no pinning forces hold the magnetic flux inside the superconductor. Max von Laue later called the discovery of the Meissner-Ochsenfeld effect a turning point in the history of superconductivity.

Based on the Meissner-Ochsenfeld effect, the energy difference between the normal (nonsuperconducting) and the superconducting state can also be calculated precisely, as Gorter and Casimir were also the first to recognize. We will briefly explain their train of thought. In the presence of a magnetic field H, the density G_s of free Gibbs energy in the superconducting state is

$$G_s(T, H) = G_s(T, 0) - \int_0^H M(H)\, dH. \tag{2.1}$$

Here M(H) is the magnetization. In the case of perfect diamagnetism due to the Meissner-Ochsenfeld effect

$$M(H) = -\frac{1}{4\pi}H. \tag{2.2}$$

$\int_0^H M(H)\, dH$ in Eq. (2.1) contains the work done in expelling the magnetic field. Together with Eq. (2.2), this results in

$$G_s(T, H) = G_s(T, 0) + \frac{1}{8\pi}H^2. \tag{2.3}$$

In equilibrium, however, the following applies to the case $H = H_C(T)$: $G_n(T, H_C) = G_s(T, H_C)$ and $G_n(T, H_C) = G_n(T, 0)$. The difference between the energy density in the normal (G_n) and superconducting state is therefore in the case $H = H_C$

$$G_n(T, 0) - G_s(T, 0) = \frac{1}{8\pi}H_C^2(T). \tag{2.4}$$

For a typical value of the critical magnetic flux density $B_C = 10^{-2}$ T, the difference in energy density is 398 erg/cm^3 $= 2.49 \cdot 10^{14}$ eV/cm^3. It is this very small value of the energy difference in the range of only a few meV per electron that has long delayed the theoretical explanation of superconductivity.

The expulsion of the magnetic field in the Meissner-Ochsenfeld effect is caused by electrical shielding currents flowing along the surface of the superconductor. They generate a magnetic field that is exactly opposite to the original magnetic field and compensates it exactly. In order for this state to persist for any length of time, these "shielding currents" must flow without electrical resistance. Superconductivity is therefore necessary (In normal, nonsuperconducting metals, only the so-called electromagnetic skin effect remains).

We recognize the special significance of the Meissner-Ochsenfeld effect from the fact that the loss-free flowing shielding currents require the phenomenon of superconductivity as a necessary consequence. However, the reverse conclusion that the existence of the Meissner-Ochsenfeld effect follows from the disappearance of the electrical resistance is not admissible. Therefore, the Meissner-Ochsenfeld effect is the decisive "fingerprint" for superconductivity.

3 London Theory, Magnetic Penetration Depth, Intermediate State

A first phenomenological theory of superconductivity and the Meissner-Ochsenfeld effect was developed by the brothers Fritz and Heinz London in 1935. In particular, their theory provides a value for the so-called magnetic penetration depth, within which the electric shielding currents flow along the surface of the superconductor and the magnetic field still exists in the superconductor. In the following, we refer to the magnetic penetration depth with the symbol λ_m.

The brothers Fritz and Heinz London had had to leave Germany as Jews after the National Socialists took over the government and were initially accepted in England. At the Clarendon Laboratory in Oxford, they then contributed (together with other emigrants from Germany) to Oxford's international leadership in the field of physics at low temperatures.

For a short description of the London theory, we start with the equation of the forces acting on an electron in the electric field **E**

$$m\frac{\partial \mathbf{v_s}}{\partial t} = (-e)\ \mathbf{E} \tag{3.1}$$

In Eq. (3.1), a dissipative contribution was neglected. The superconducting current density

$$\mathbf{j}_s = (-e)\ n_s\ \mathbf{v}_s \tag{3.2}$$

yields the relationship

$$\mathbf{E} = \left[m/\left(e^2\ n_s\right)\right]\frac{\partial \mathbf{j_s}}{\partial t} = \mu_o\lambda_m^2\frac{\partial \mathbf{j_s}}{\partial t}. \tag{3.3}$$

R. P. Huebener, *History and Theory of Superconductors,* Springer essentials,
https://doi.org/10.1007/978-3-658-32380-6_3

In Eq. (3.3), we introduced the magnetic penetration depth λ_m, which is defined by

$$\lambda_m^2 = m/(\mu_o\, n_s\, e^2) \tag{3.4}$$

Here m is the mass, n_s the density and $\mathbf{v}_s$ the velocity of the superconducting electrons. μ_o is the vacuum permeability.

Since the superconducting shielding current exactly compensates an external magnetic field, the Maxwell equation

$$\text{curl}\ \mathbf{H} = \mathbf{j} \tag{3.5}$$

is a good approximation of the maximum density j_s of the shielding current

$$j_s = H_C/\lambda_m. \tag{3.6}$$

On the other hand, the Maxwell equation ($\mathbf{B}$ = magnetic flux density) yields

$$\text{curl}\ \mathbf{E} = -\frac{\partial \mathbf{B}}{\partial t} \tag{3.7}$$

together with Eq. (3.3)

$$\mu_o \lambda_m^2 \text{curl}\left(\frac{\partial \mathbf{j_s}}{\partial t}\right) + \frac{\partial \mathbf{B}}{\partial t} = 0. \tag{3.8}$$

By suppressing the time derivative in Eq. (3.8), Fritz and Heinz London postulated a new equation

$$\mu_o \lambda_m^2\, \text{curl}\ \mathbf{j}_s + \mathbf{B} = 0. \tag{3.9}$$

The Maxwell Eq. (3.5) and the relation curl curl $\mathbf{x}$ = grad div $\mathbf{x} - \Delta\, \mathbf{x}$ finally results in

$$\Delta \mathbf{H} = \frac{1}{\lambda_m^2}\mathbf{H} \tag{3.10}$$

with the solution

$$\mathbf{H}(x) = \mathbf{H}(0)\ \exp\,(-x/\lambda_m). \tag{3.11}$$

In Fig. 3.1, we show the course of the magnetic field H_0 and the density n_s of the superconducting electrons in the vicinity of the interface between a normal conductor (N) and a superconductor (S). Here we have assumed the geometry of a superconductor whose x-coordinate runs from the surface at $x = 0$ *left* to the inside of the superconductor and which fills the (left) half space $x>0$. The magnetic field **H** is assumed perpendicular to the x-direction.

Today, Eqs. (3.3) and (3.9) are known as the first and second London equations. They characterize superconductors in contrast to other materials. Physically, Eq. (3.11) means that an external magnetic field inside a superconductor decays exponentially, with the decay occurring within a surface layer of the thickness λ_m. The limiting case $T \to T_C$ results in $n_s \to 0$ and therefore $\lambda_m \to \infty$.

Typical values of the magnetic penetration depth are in the range $\lambda_m = 40 - 60$ nm. As an important material-specific spatial length, the magnetic penetration depth plays a role in many properties of superconductors.

After the London theory established the fundamental importance of the magnetic penetration depth in superconductors, the Englishman Alfred Brian Pippard pointed out for the first time in 1950 that the superconducting property cannot change abruptly in space and has a certain spatial rigidity. This is expressed by the so-called coherence length ξ. Changes in the superconducting properties are only possible at spatial distances greater than the coherence length. This fact is explained by the Ginzburg–Landau theory, which also dates from 1950. The theory is named after the two Russians Vitaly Lazarevich Ginzburg and Lew Dawidowitsch Landau. In Chapter 5, we come back to this.

The two characteristic lengths λ_m and ξ play a role, for example, at the interfaces between normal and superconducting regions in the same material. Here, the finite value of the coherence length causes a superconducting region to lose its superconducting property and the associated condensation energy density (Eq. (2.4)) already at the distance ξ in front of this interface, thus making a positive contribution $\alpha_1 = (H_C^2/8\pi)\xi$ to the interface energy. However, since no gain and therefore no loss of condensation energy occurs within the magnetic penetration depth λ_m, the value $(H_C^2/8\pi)\lambda_m$ must still be deducted from this. Finally, for the wall energy of an interface between a normal and a superconducting region, one finds

$$\alpha = (H_C^2/8\pi)(\xi - \lambda_m). \tag{3.12}$$

In Fig. 3.1, we show the spatial impact of the two lengths ξ and λ_m. In connection with this result Eq. (3.12), it was assumed that the interfacial energy must always be positive and $\xi > \lambda_m$ must therefore apply.

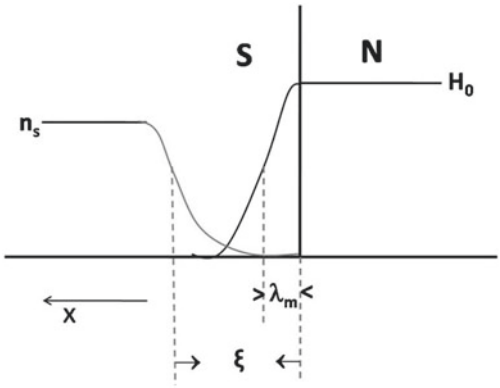

Fig. 3.1 Dependence of the density of superconducting electrons, n_s, and the magnetic field H on the distance from the interface between a normal (N) and a superconducting (S) region. The x-coordinate runs in the superconductor from the surface at $x = 0$ *left* to the interior of the superconductor

When discussing the Meissner-Ochsenfeld effect, we had previously not considered the so-called demagnetization effect. This effect is based on the fact that the magnetic field expulsion increases the magnetic field in the immediate vicinity of the superconductor. This behavior is quantified by the so-called demagnetization coefficient D of the geometry of the superconductor. If we call the magnetic field at the edge of the superconductor H_R, the following applies

$$H_R = H/(1 - D) \tag{3.13}$$

The coefficient D depends on the geometry and varies in the range 0–1. From Eq. (3.13), we can see that in the range

$$H_C\ (1 - D)\ <\ H\ <\ H_C \tag{3.14}$$

the case $H_R > H_C$ is present and superconductivity must be interrupted. In Table 3.1, we have compiled the demagnetization coefficient D for some geometries.

From Table 3.1, we can see that in the case of a thin plate or cylinder oriented parallel to H, the magnetic field in the outer space is hardly changed by the field expulsion. On the other hand, we expect a large field increase in the case of a plate oriented perpendicular to H, so that the magnetic field at the outer edge quickly becomes larger than the critical magnetic field $H_C(T)$.

In the range marked by Eq. (3.14), superconductivity can no longer be maintained everywhere, and magnetic flux must penetrate the superconductor. In 1937, Landau proposed the existence of a new "*intermediate state*" for this case, in which normal domains with the local magnetic field H_C and superconducting

Table 3.1
Demagnetization coefficient D for different geometries

Geometry	D
Thin plate oriented parallel to H	≈0
Thin cylinder oriented parallel to H	≈0
Sphere	1/3
Cylinder oriented perpendicular to H with circular	1/2
Cross section	
Thin plate oriented perpendicular to H	≈1.0

domains with the local magnetic field zero exist. According to Eq. (3.12), we expect for these domains a wall energy proportional to the length difference $\xi - \lambda_m$, where $\xi > \lambda_m$.

In Fig. 3.2, we show the intermediate state of a superconducting lead layer of 9.3 μm thickness at 4.2 K for different values of the magnetic field oriented perpendicular to the layer. The images were obtained magneto-optically using a polarization microscope. The normal domains are bright and the superconducting domains are dark. The critical magnetic field of lead at 4.2 K is 550 G (T_C = 7.2 K).

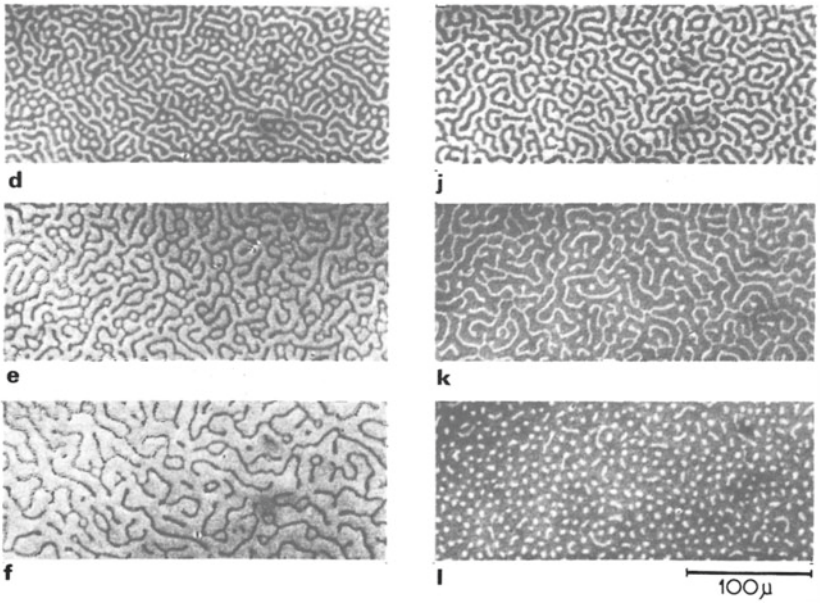

Fig. 3.2 Intermediate state of a superconducting lead layer of 9.3 μm thickness at 4.2 K in rising (**d–f**) and falling (**j–l**) perpendicular magnetic field for the following magnetic field values: **d** 218 G; **e** 348 G; **f** 409 G; **j** 260 G; **k** 101 G; **l** 79 G. Normal domains are bright, superconducting domains are dark

4 Type II Superconductors, Abrikosov Vortex Lattice, Mixed State

As early as the 1930s, experiments, particularly those by Leo Vasilyevich Shubnikov in Kharkov in Soviet Ukraine, showed that the ideas of that time in the field of superconductivity needed to be expanded. Shubnikov had built a low-temperature laboratory there early on, in which experiments could also be carried out with liquid helium. (However, Shubnikov's many foreign contacts became his undoing during the Stalin terror of the time. Stalin had him arrested and shot on November 10, 1937, after 3 months in custody).

Electrical and magnetic measurements, especially on superconducting alloys, had shown behavior that was not understood at that time. Especially the question of the relative size of the coherence length ξ and the magnetic penetration depth λ_m came into focus. The young theoretical physicist Alexei A. Abrikosov at the University of Moscow made the decisive breakthrough at that time. He was a friend of Nikolay Zavaritskii, who wanted to verify the predictions of the Ginzburg–Landau theory at the Kapitza Institute for Physical Problems by means of experiments on superconducting thin films. Until then, the only case in which the length difference ξ–λ_m, and thus also the wall energy during domain formation in superconductors, was positive, had been considered.

Abrikosov and Zavaritskii now seriously discussed for the first time the possibility that the length difference can also become negative if the coherence length ξ is smaller than the magnetic penetration depth λ_m. Based on the Ginzburg–Landau theory, Abrikosov calculated the critical magnetic field for this case as well. He was able to prove that this was the only way to achieve good agreement with Zavaritskii's experimental data for particularly carefully prepared thin films. Abrikosov and Zavaritskii were now convinced that they had discovered a new type of superconductor, which they called the "second group." Today, this group is called type II superconductors (with $\xi < \lambda_m$), while the superconductors with positive wall energy are called type I superconductors (with $\xi > \lambda_m$).

R. P. Huebener, *History and Theory of Superconductors,* Springer essentials,
https://doi.org/10.1007/978-3-658-32380-6_4

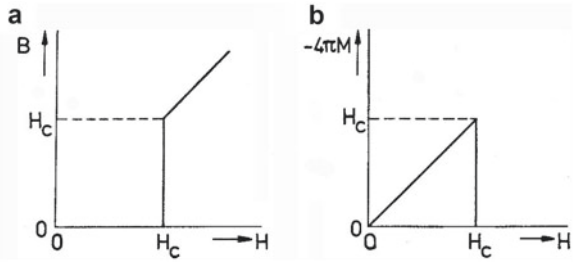

Fig. 4.1 **a** Magnetic flux density B and **b** magnetization $-4\pi M$ as a function of the applied magnetic field H in the case of a type I superconductor

His further theoretical analysis of type II superconductors using the Ginzburg–Landau theory led Abrikosov to discover a novel state in the presence of a magnetic field: The superconductor may be permeated by a regular lattice of individual magnetic flux quanta. Abrikosov had found the flux line lattice and the so-called mixed state. How revolutionary Abrikosov's discovery was at that time can be seen from the fact that his doctoral supervisor, Lew Dawidowitsch Landau, did not agree with the novel result. Only after the American Richard Phillips Feynman, only a few years later, also discussed quantized vortex lines in rotating superfluid helium, did Landau give his consent. In this way, the publication of Abrikosov's work, which was completed in 1953, was delayed by several years.

The magnetic flux quanta that permeate the superconductor like filaments are generated by superconducting ring currents, which generate a spatially confined, local magnetic field like a magnet coil. We will come back to the magnetic flux lines in Chap. 5.

In Fig. 4.1, we show once again the magnetic flux density B inside a type I superconductor and its magnetization M as a function of the applied magnetic field H for the case of a geometry with a vanishing demagnetization coefficient D. We see the perfect diamagnetism with $B = 0$ below the critical magnetic field H_C and the linear increase of $-4\pi M$ with increasing H.

The superconducting mixed state with the magnetic flux line lattice exists in the region of the magnetic field above the "lower critical magnetic field" $H_{C1} < H_C$ and below the "upper critical magnetic field" H_{C2}, i.e., in the region $H_{C1} < H < H_{C2}$. Below H_{C1}, the Meissner-Ochsenfeld effect still applies. In Fig. 4.2, this behavior is shown schematically (again under the assumption $D \approx 0$).

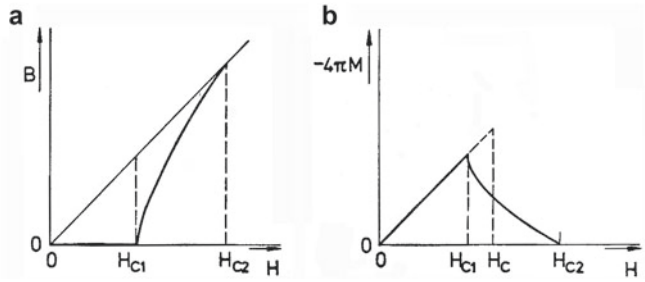

Fig. 4.2 **a**Magnetic flux density B and **b** magnetization $-4\pi M$ as a function of the applied magnetic field H in the case of a type II superconductor

The first experimental proof of the magnetic flux line lattice was performed by elastic neutron diffraction in 1964 on the basis of the interaction of the magnetic moment of the neutrons with the magnetic field gradients of the mixed state. A particularly impressive experimental confirmation was achieved in 1967 by Uwe Essmann and Hermann Träuble using the so-called Bitter technique. They sprinkled a fine ferromagnetic powder onto the surface of the superconductor. There the powder is attracted by the points where the magnetic flux lines reach the surface. The small heaps of powder that are formed thus decorate the individual flux lines (Fig. 4.3).

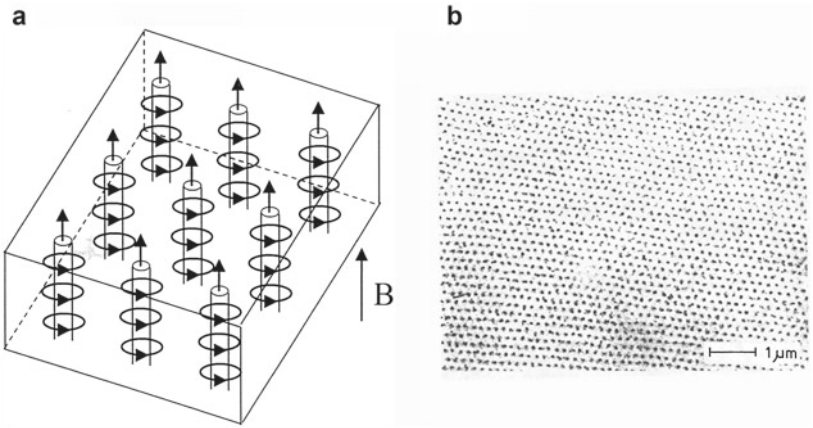

Fig. 4.3 Superconducting mixed state with the lattice of quantized magnetic flux lines proposed by Abrikosov for the first time. **a** Schematic diagram. A total of nine magnetic flux lines are shown, each magnetic flux line being surrounded by superconducting ring currents. **b** Experimental proof of the Abrikosov lattice of magnetic flux lines for a 0.5-mm thick plate of superconducting niobium by decoration with the Bitter technique. The many dark dots mark the places where the individual magnetic flux lines penetrate the surface of the superconducting plate. (U. Essmann)

5 Ginzburg–Landau Theory, Magnetic Flux Quantization, London Model

The phenomenological Ginzburg–Landau theory on which Abrikosov based his theory describes the electrons in the superconducting state by a macroscopic wave function

$$\psi(\mathbf{r}, t) = |\psi(\mathbf{r}, t)|\, e^{i\varphi(\mathbf{r},t)} \tag{5.1}$$

with an amplitude $|\psi(\mathbf{r}, t)|$ and a phase $\varphi(\mathbf{r}, t)$. The complex wave function $\psi(\mathbf{r}, t)$ can be interpreted in the sense of Landau as order parameter of a phase transition. The absolute value $|\psi(\mathbf{r}, t)|$ is linked to the local density $n_s(\mathbf{r})$ of the superconducting electrons, $|\psi(\mathbf{r}, t)|^2 = n_s$. The phase of the order parameter $\varphi(\mathbf{r}, t)$ provides the description of the superconducting currents.

In the theory, the density G of the free energy of the electrons is expanded according to powers of the order parameter. An important assumption here is that $\psi(\mathbf{r}, t)$ has only small values. Thus, strictly speaking, the theory is only applicable just below T_C. Taking into account spatial variations of the order parameter and an existing magnetic field with the flux density $\mathbf{B} = \text{curl}\ \mathbf{A}$ ($\mathbf{A}$ = vector potential), the expansion of the free energy density is

$$G = G_n + \alpha(T)|\psi|^2 + \frac{\beta(T)}{2}|\psi|^4 + \frac{1}{2m^*}\left|\left(\frac{\hbar}{i}\nabla - \frac{e^*}{c}\mathbf{A}\right)\psi\right|^2 + B^2/8\pi \tag{5.2}$$

m^* is the mass and e^* the charge of the particles (c = speed of light). Equation (5.2) is the starting point of the Ginzburg–Landau theory. From the expression (Eq. (5.2)) for the free energy density, the minimum value must be found with spatial variation of the order parameter $\psi(\mathbf{r})$ and the magnetic field or the vector potential $\mathbf{A}(\mathbf{r})$. With the help of a common variation method, one finds the two

R. P. Huebener, *History and Theory of Superconductors,* Springer essentials,
https://doi.org/10.1007/978-3-658-32380-6_5

differential equations according to Ginzburg–Landau

$$\alpha\ \psi + \beta\ |\psi|^2\ \psi + \frac{1}{2\mathrm{m}^*}\left(\frac{\hbar}{i}\nabla - \frac{\mathrm{e}^*}{\mathrm{c}}\mathbf{A}\right)^2 \psi = 0 \tag{5.3a}$$

$$\mathbf{j}_\mathrm{s} = \frac{e^*\hbar}{2m^*i}(\psi^*\nabla\,\psi - \psi\nabla\,\psi^*) - \frac{e^{*2}}{m^*c}\psi^*\psi\ \mathrm{A} \tag{5.3b}$$

Equation (5.3a) has the form of a Schrödinger equation with the eigenvalue $-\alpha$ of energy. The contribution $\beta\ |\psi|^2\ \psi$ acts like a repulsive potential. Equation (5.3b) is the quantum mechanical description of a particle current. Both equations apply to particles of mass m^* and charge e^*.

Abrikosov's discovery of the magnetic flux line lattice was a great success for the Ginzburg–Landau theory. The description of the superconducting state of the electrons by a macroscopic quantum mechanical wave function had proved to be particularly fruitful. Important results are the explanation of the characteristic lengths $\xi(\mathrm{T})$ and $\lambda_\mathrm{m}(\mathrm{T})$, the critical electric current density $\mathrm{j_c}$ and magnetic flux quantization.

The smallest possible unit of magnetic flux in a superconductor is the magnetic flux quantum $\mathrm{h/2e} = 2.068 \cdot 10^{-15}$ V s. The quantity h is Planck's constant and e the charge of an electron. This quantization condition follows from the fact that the macroscopic wave function describing the superconducting state has to reproduce itself exactly if one moves with the spatial coordinate point of the wave function once around the enclosed magnetic flux region and returns to the starting point. Experimentally, magnetic flux quantization was first demonstrated in 1961 by Robert Doll and Martin Näbauer and independently by Bascom Deaver and William Fairbank. With the help of a small superconducting tube of only about 10 μm diameter (a superconducting lead cylinder vapor-deposited on a quartz filament) placed in a low magnetic field parallel to the axis of the tube, Doll and Näbauer were able to show that the magnetic flux present in the small hollow cylinder was either zero or an integer multiple of the flux quantum mentioned above (Fig. 5.1).

A more detailed explanation of the step structure shown in Fig. 5.1b can be found in Fig. 5.2. Part a shows the superconducting shielding current $\mathrm{I_s}$ as a function of the magnetic flux density $\mathrm{B_e}$, which is parallel to the axis of the small superconducting cylinder. The magnetic flux passing through the cross-sectional area of the cylinder is $\pi\mathrm{R}^2\mathrm{B_e}$ (R = cylinder radius) and is given in units of the magnetic flux quantum $\varphi_\mathrm{o} = \mathrm{h/2e}$ (the vector $\boldsymbol{\varphi}_\mathrm{o}$ is oriented parallel to the direction of the flux density **B**).

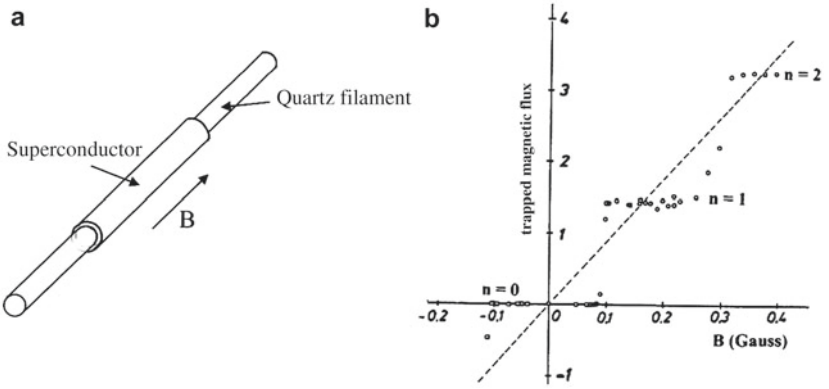

Fig. 5.1 Experimental proof of magnetic flux quantization in a superconductor. **a** The tube consisting of a superconductor of only about 10 μm diameter is cooled in a magnetic field B oriented parallel to its axis. Below the critical temperature T_C, the magnetic field is switched off and the frozen magnetic flux in the tube is measured. **b** As a function of the magnetic field B, the frozen magnetic flux shows a quantized step structure, since only integer multiples of the magnetic flux quantum (h/2e) are allowed in the tube. The figure shows the observation of 0, 1 and 2 magnetic flux quanta. Without quantization, the measuring points should lie on the dotted straight line. (R. Doll and M. Näbauer)

The shielding current I_s shown in Fig. 5.2 initially prevents magnetic flux from entering the cylinder opening due to the Meissner-Ochsenfeld effect. At the value $B_e = \varphi_o/(2\pi R^2)$ of the magnetic flux density the shielding current compensates exactly half a flux quantum $\varphi_o/2$ in the cylinder (point (1)). If B_e is further increased, the shielding current I_s changes its sign and thus causes exactly one flux quantum φ_o to exist in the cylinder. One half of the flux quantum is generated by I_s (point (2)). If B_e is now increased further, $|I_s|$ decreases again until $B_e = \varphi_o/(\pi R^2)$ reaches the state with $I_s = 0$ (point (3)). This process is repeated with further increase of B_e. In the cylinder, the steps with the number n of magnetic flux quanta thus come about (Figs. 5.1b and 5.2b). In Fig. 5.2c, the superposition of the applied magnetic field (solid arrows) and the magnetic field generated by I_s (dashed arrows) is shown schematically for the three points (1) to (3) from Fig. 5.2a. Due to the entry of the magnetic flux quanta φ_o into the cylinder, the shielding current I_s and the kinetic energy associated with it remains limited instead of increasing indefinitely.

A physical description of the magnetic flux line in a type II superconductor, which Abrikosov discussed for the first time, is provided by the *London model.*

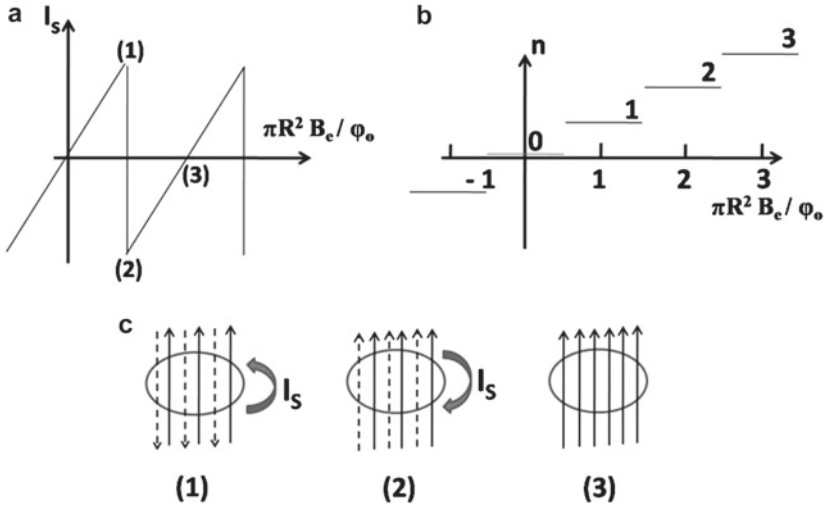

Fig. 5.2 Experimental demonstration of magnetic flux quantization at the entry of magnetic flux into a small superconducting cylinder. Part **a** shows the superconducting shielding current I_s as a function of the magnetic flux density B_e oriented parallel to the cylinder axis. Part **b** gives the number n of magnetic flux quanta in the cylinder as a function of B_e. Part **c** explains the superposition of the applied magnetic field (solid arrows) and the magnetic field generated by I_s (dashed arrows) at the three points (*1*) to (*3*). Further details can be found in the text

The model assumes a normal vortex core with the radius ξ embedded in the superconducting phase. The radius ξ of the normal vortex core is assumed to be small compared to the magnetic penetration depth λ_m, $\xi \ll \lambda_m$. The ratio λ_m/ξ is defined as the *Ginzburg–Landau parameter* κ, which is highly important for superconductivity

$$\kappa = \lambda_m/\xi \tag{5.4}$$

The London model is a good approximation in the range $H_{C1} < H \ll H_{C2}$, where the interaction between the flux lines is not yet too strong.

In the case of an isolated single flux line, i.e., in the case of a magnetic field only slightly above H_{C1}, the flux lines are far apart and their interaction can be neglected. The schematic Fig. 5.3 shows the structure of an isolated flux line. The local magnetic field **h** in the vicinity of the flux line reaches its maximum

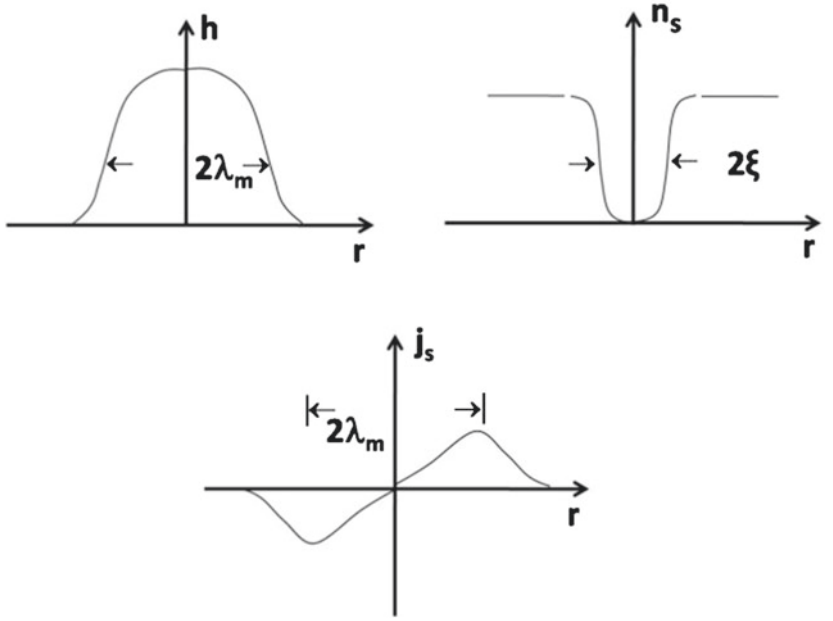

Fig. 5.3 Structure of a single flow line. Local magnetic field **h**, density of the superconducting electrons n_s, and the circulating superconducting current density j_s as a function of the distance r from the axis of the flux line

in the center and decreases exponentially with increasing distance from the center, approximately outside the radius λ_m. The density n_s of the superconducting electrons is suppressed to zero at the center of the flux line and reaches its full value outside the radius ξ. The density j_s of the circular current, which generates the magnetic field **h**(**r**) of the flux line, reaches its maximum at about the radius λ_m and vanishes in the normal vortex core. For the mean magnetic flux density **B,** we have the important relationship.

$$\mathbf{B} = n\ \varphi_0, \tag{5.5}$$

where n is the vortex density (number of vortices per area).

From the London model, the electric super-current density j_s as well as the local magnetic flux density h(r) in the vicinity of a magnetic flux line, the energy per unit length of a flux line, the lower critical field H_{C1}, the interaction between

the magnetic flux lines and the magnetization in the vicinity of H_{C1} can be calculated. However, the simplicity of this useful phenomenological theory is gained only by the unrealistic behavior of the expressions with their divergence on the axis of the flux line. This divergence can be avoided by cutting off the area of the vortex core at $r < \xi$ during integration.

BCS Theory, Energy Gap

6

A theoretical explanation of superconductivity was sought early on. Albert Einstein, for example, had suggested that superconductivity is caused by molecular chains (similar to Ampère's molecular currents). In a manuscript of March 1922 entitled "*Theoretical Remarks on the Superconductivity of Metals*" (*Theoretische Bemerkungen zur Supraleitung der Metalle*; published in September 1922), Einstein had discussed the superconducting state as follows:

> It therefore seems inevitable that the superconducting currents are carried by closed molecular chains (conduction chains), whose electrons constantly undergo cyclic permutations. Kamerlingh Onnes therefore compares the closed currents in superconductors with Ampère's molecular currents. … It may be regarded as improbable that different kinds of atoms can form conducting chains with each other. So perhaps the transition from one superconducting metal to another is never superconducting.

However, Kamerlingh Onnes was already interested in the contact between two different superconductors. At the end of the mentioned manuscript, Albert Einstein writes in a short P.S.: "*The last hinted assumptions … are partly disproved by an important experiment, which Kamerlingh Onnes carried out in the last months. He showed that at the contact point of two different superconductors (lead and tin), no measurable ohmic resistance appears.*"

The question of the behavior of a contact between two superconductors was taken up again in 1932, when Walther Meissner showed in experiments together with Ragnar Holm that the mechanical contact between two superconductors is also superconducting, which is incompatible with molecular chains. We will come back to the contact between two superconductors in Chapter 7 when discussing the Josephson effect.

R. P. Huebener, *History and Theory of Superconductors,* Springer essentials,
https://doi.org/10.1007/978-3-658-32380-6_6

Phenomenological theories such as the London theory and the Ginzburg–Landau theory meant important stations in theoretical understanding. However, a microscopic explanation of the mechanism was still missing. The list of those who had tried this is long. Besides Albert Einstein, we mention the names of Felix Bloch, Niels Bohr, Léon Brillouin, Jakov I. Frenkel, Werner Heisenberg, Ralph Kronig, Lew Dawidowitsch Landau and Wolfgang Pauli.

In 1957, John Bardeen, Leon Cooper and Robert Schrieffer achieved a decisive progress. Their "BCS theory" was quickly accepted. The reason why it took so long to find a convincing theoretical explanation of superconductivity is that the energy difference of the electrons between their normal and superconducting states is extremely small and much smaller than the Fermi energy. However, the calculation of the various individual contributions to the energy of the electrons in the crystal is much less accurate than the energy gain achieved during the transition to the superconducting state.

The BCS theory is based on the idea that at low temperatures, there is an attractive force between two electrons, so that two electrons combine to form pairs in a certain way. The binding energy thus obtained leads to a reduction in energy. Leon Cooper had already theoretically deduced such pair formation and energy lowering in 1956. Therefore, the pairs of electrons are called "Cooper pairs." The attraction during the formation of the Cooper pairs is caused by distortions of the crystal lattice in the vicinity of the individual electrons. Phonons therefore play a role here.

Herbert Fröhlich and independently John Bardeen had developed an important basic idea for this in 1950. They had realized that an electron distorts the crystal lattice in its environment. Due to the electron–phonon interaction, an electron moving through the crystal lattice is surrounded by a cloud of virtual phonons, which are continuously emitted and reabsorbed. The formation of Cooper pairs is due to the exchange of virtual phonons between the two electrons. This process is shown schematically in Fig. 6.1. An electron with the wave vector $\mathbf{k}$ emits a virtual phonon $\mathbf{q}$, which is absorbed by an electron $\mathbf{k'}$**.** The virtual phonon scatters $\mathbf{k}$ to $\mathbf{k} - \mathbf{q}$ and $\mathbf{k'}$ to $\mathbf{k'} + \mathbf{q}$**.** Since the process is virtual, energy conservation does not have to be maintained. The exchange of phonons between the electrons leads to an attraction when one of the electrons is surrounded by a positive shielding charge through the lattice, which overcompensates the negative elementary charge. The other electron is then attracted by the net positive charge.

Experimental observations of the so-called isotope effect had already indicated the important role of the crystal lattice in superconductivity in the early 1950s. The term isotope effect is used when the result depends on the mass of the atomic nuclei at constant electric charge of the nuclei, i.e., on the number of neutrons in

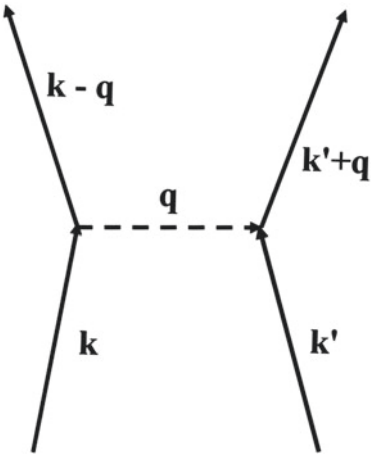

Fig. 6.1 Exchange of a virtual phonon **q** between the electrons with the wave vectors **k** or **k′**

the atomic nucleus. In various specially produced isotopically pure superconducting metals (lead, mercury, and tin), it was found that the critical temperature T_C is inversely proportional to the square root of the mass M of the lattice atoms:

$$T_c \sim 1/M^{\alpha} \tag{6.1}$$

The exponent was $\alpha = 0.5$. The crystal lattice therefore had to play a role in superconductivity.

The Cooper pairs always consist of two electrons with oppositely directed intrinsic angular momentum, so that the total spin of the individual Cooper pair disappears. In this case, the Pauli principle is invalid and all Cooper pairs can occupy the same quantum state. This quantum state is described by a macroscopic quantum mechanical wave function. However, the formation of Cooper pairs and the macroscopic quantum state is restricted to a certain small energy range in the vicinity of the Fermi surface (and thus to a small part of the conduction band).

At the heart of the BCS theory is the idea of an energy gap in the energy spectrum of electrons at the Fermi energy. Above the critical temperature T_C, the energy gap disappears, and below T_C, it grows in a certain way as the temperature decreases, reaching its maximum at 0 K. First indications of a gap in the energy spectrum of the electrons had already been obtained by optical absorption experiments on superconducting thin films. In 1960, Ivar Giaever provided impressive proof of the energy gap through his famous tunnel experiment (Fig. 6.2). At that time, he had been particularly fascinated by the quantum mechanical tunneling

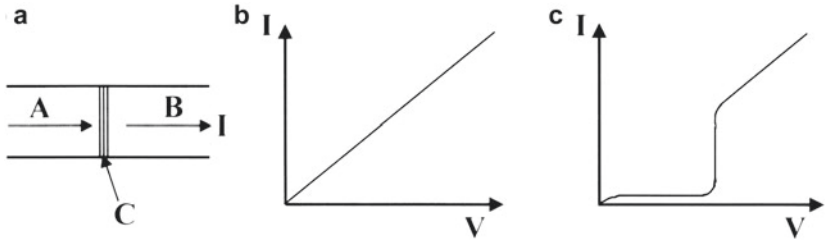

Fig. 6.2 Experimental proof of the energy gap in a superconductor by the tunnel experiment of Giaever. **a** A superconducting electrode A and a normal electrode B are separated from each other by a thin, electrically insulating barrier C, so that the flow of electric current through the barrier is only possible by the quantum mechanical tunnel effect. **b** Electric current I as a function of voltage V, when both electrode metals are in the normal state. **c** Electrical current I as a function of the voltage V, if one metal electrode is superconducting. Only when the potential difference between the two electrodes has reached the value of the energy gap can the electric current flow begin

process for quite some time. After hearing about the new BCS theory and its prediction of a gap in the energy spectrum of electrons, he succeeded in demonstrating the energy gap directly by means of the electric current flow between a superconducting and a normal electrode: If the two electrodes are separated from each other by a thin electrically insulating barrier, the electric current flow can only come about through the quantum mechanical tunnel effect. In such a "tunnel contact," the wave function of the particles extends to the other side of the barrier. However, the tunnel current cannot yet flow if no permitted energy states are available on the other side in the superconductor. The electric current only begins to flow when the potential difference between the two sides of the contact has reached the value of the energy gap. If both electrodes are superconducting, it is similar. In this way, Giaever succeeded in determining the energy gap with a simple measurement of electrical voltage and electrical current. Such tunnel experiments on superconductors have subsequently become very important.

The formation of Cooper pairs in superconductivity is also expressed in the size of the magnetic flux quantum discussed above. Since the Cooper pairs consist of two elementary charges, it follows that the magnetic flux quantum $\varphi_o = h/2e$ is only half as large as in the case where only a single elementary charge is involved.

Josephson Effect

7

The contact between two superconductors, which we mentioned at the beginning of Chapter 6 in connection with Kamerlingh Onnes and Walther Meissner, was to take on a prominent role about three decades later. After Ivar Giaever had published the results of his famous tunnel experiment to prove the energy gap in superconductors, the student Brian David Josephson in Cambridge, England, became interested in the underlying tunneling process. He had heard about the new BCS theory in lectures and was particularly impressed by the concept of superconductivity as a macroscopic quantum phenomenon. He theoretically investigated the flow of electric current through the barrier of a tunnel contact between two superconductors, as Giaever had also used it. He derived two equations for the electric current and for the electric voltage, which have since been known as Josephson equations:

$$I_s = I_C \sin \chi \tag{7.1}$$

$$\frac{\partial \chi}{\partial t} = \frac{2e}{\hbar} V \tag{7.2}$$

In Eq. (7.1), the supercurrent flowing without electrical resistance is described by Cooper pairs. Equation (7.2) states that an electric voltage V at the tunnel contact is always accompanied by an alternating supercurrent oscillating at high frequency between the two superconductors. The frequency of this Josephson oscillation increases in proportion to the electrical voltage. Equations (7.1) and (7.2) are based on the concept that superconductivity is a macroscopic quantum phenomenon described by the wave function (order parameter) Eq. (5.1) with an amplitude $|\psi(\mathbf{r}, t)|$ and a phase $\varphi(\mathbf{r}, t)$. In Eq. (7.1), χ denotes the phase difference $\chi = \varphi_2 - \varphi_1$ between both sides of the contact. The supercurrent I_s

R. P. Huebener, *History and Theory of Superconductors,* Springer essentials,
https://doi.org/10.1007/978-3-658-32380-6_7

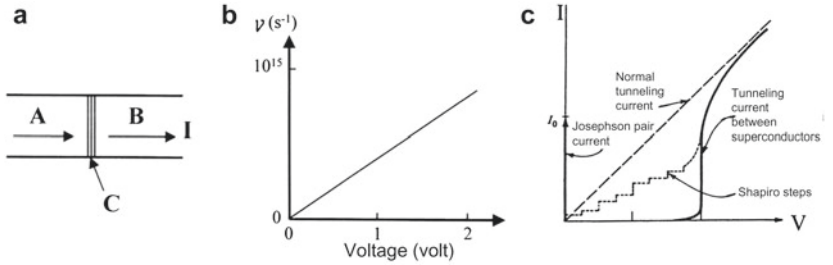

Fig. 7.1 Josephson oscillation of the supercurrent between the superconducting electrodes of a tunnel contact in the presence of an electrical voltage at the contact. **a** In the Josephson contact, the two superconducting electrodes A and B are only weakly coupled to each other, for example, by a thin, electrically insulating barrier C, which still allows electrical current to flow through the quantum mechanical tunneling process. **b** The frequency ν of the Josephson oscillation of the supercurrent between the two electrodes increases proportionally to the electrical voltage V at the contact. At the voltage of 1 V, the frequency is approximately 483,000 GHz. **c** Electric current I as a function of the voltage V for a Josephson contact. The solid curve shows the tunnel current for superconductivity and the dashed straight line shows the tunnel current for normal conduction. At voltage zero, the Josephson pair current can be seen up to its maximum value I_0. When the contact is irradiated with microwaves, the curve shows "Shapiro steps" caused by the interaction of the Josephson oscillation in the contact with the microwaves

flowing through the contact is given by the sine function of this phase difference $\chi = \varphi_2 - \varphi_1$. I_C denotes the critical current of this contact geometry.

The Josephson Eqs. (7.1) and (7.2) can be derived in different ways. A derivation by Richard Feynman starts with the time-dependent Schrödinger equation for the two wave functions ψ_1 and ψ_2 for the initially still separate superconductors 1 and 2 and adds a coupling between the two.

Josephson made his predictions in 1962 but his theory was initially met with skepticism and incomprehension. It was experimentally confirmed as early as 1963 (Fig. 7.1). The second Josephson equation again manifests the double elementary charge of the Cooper pairs responsible for superconductivity.

8 Movement of the Flux Quanta, Flux Flow Resistance

The question of how exactly the electrical resistance in superconductivity disappears to zero came into focus in the early 1960s, when newly discovered superconductor materials first appeared to make their technical applications at high electrical currents possible. Especially, the new superconducting niobium alloys Nb_3Sn and NbZr were very promising. Careful measurements, especially at the Bell laboratories in the USA, revealed indications of high values of critical electric current density and critical magnetic field. A novel "critical state" was also found, above which a finite, albeit relatively small, electrical resistance occurs. The American Philip W. Anderson recognized at that time that a new process must be involved, namely a movement of magnetic flux quanta caused by the flow of electric current. This process then became famous as "flux creep" and "flux flow."

Every movement of magnetic flux quanta in a superconductor due to a force acting on them generates an electric field in the superconductor and thus an electric voltage. This "flux flow voltage" grows proportionally to the speed and number of moving flux lines. In the case of an electric current of density **j,** the Lorentz force $\mathbf{f}_L = \mathbf{j} \times \boldsymbol{\varphi}_o$ acts on the flux quanta. The Lorentz force is oriented perpendicular to the direction of the electric current and the magnetic field of the flux lines. The movement of the flux lines thus caused generates the electric field **E:**

$$\mathbf{E} = -\mathbf{v}_{\boldsymbol{\varphi}} \times \mathrm{B} \tag{8.1}$$

The magnetic flux density **B** is given by the areal density n of the magnetic flux quanta $\boldsymbol{\varphi}_o$: $\mathbf{B} = \mathrm{n}\ \boldsymbol{\varphi}_o$. The quantity $\mathbf{v}_\varphi$ denotes the velocity of the flux lines. The electric field (Eq. (8.1)) is always oriented perpendicular to the direction of motion and to the magnetic field of the magnetic flux lines. Since the electric field

R. P. Huebener, *History and Theory of Superconductors,* Springer essentials,
https://doi.org/10.1007/978-3-658-32380-6_8

and the electric current have the same direction, energy is dissipated by the flux line motion in the superconductor and electric losses occur. This process of flux motion follows the (here simplified) equation of forces

$$\mathbf{j} \times \boldsymbol{\varphi}_0 - \boldsymbol{\eta}\, \mathbf{v}_{\varphi} = 0 \tag{8.2}$$

Here $\eta\ \mathbf{v}_{\varphi}$ denotes the dissipative contribution and η a damping constant. In Eq. (8.2), the forces refer to a unit length of the flux line. From Eqs. (8.1) and (8.2), one finds the *specific flux flow resistance*

$$\boldsymbol{\rho}_{\mathrm{f}} = \boldsymbol{\varphi}_0\, \mathrm{B}/\boldsymbol{\eta} \tag{8.3}$$

This mechanism always limits the current flow without electrical resistance and losses in superconductors. Therefore, many efforts have been made to prevent this process of flux line movement as far as possible by installing so-called pinning centers. (In Eq. (8.2) we have, for the sake of simplicity, neglected the pinning forces and a force component that causes the Hall effect when the flux lines move.)

As an example we show in Fig. 8.1 the flux-flow voltage as a function of the electric current in a niobium foil for different values of the magnetic field oriented perpendicular to the foil. (thickness of the foil = 18 μm, width of the foil = 4 mm, T = 4.22 K). The electrical resistance ratio R(295 K)/R(4.2 K) was 620, where R(4.2 K) was measured in a perpendicular magnetic field of 4,000 G. The voltage starts at a finite critical current and initially shows an upwardly curved behavior. It then grows linearly with increasing current, as can be expected from Eqs. (8.1) and (8.2). The finite critical current results from the pinning forces due to spatial inhomogeneities in the superconductor, which, as pinning centers, prevent the movement of the magnetic flux lines. The slope of the linear curve sections represents the flux flow resistance and increases with increasing external magnetic field.

Figure 8.2 shows a schematic representation of the resistivity ρ_{f} as a function of the external magnetic field H. Initially, ρ_{f} grows linearly with H and then leads into a much steeper curve branch, which reaches the normal value ρ_{n} of the resistivity at the upper critical magnetic field H_{C2}.

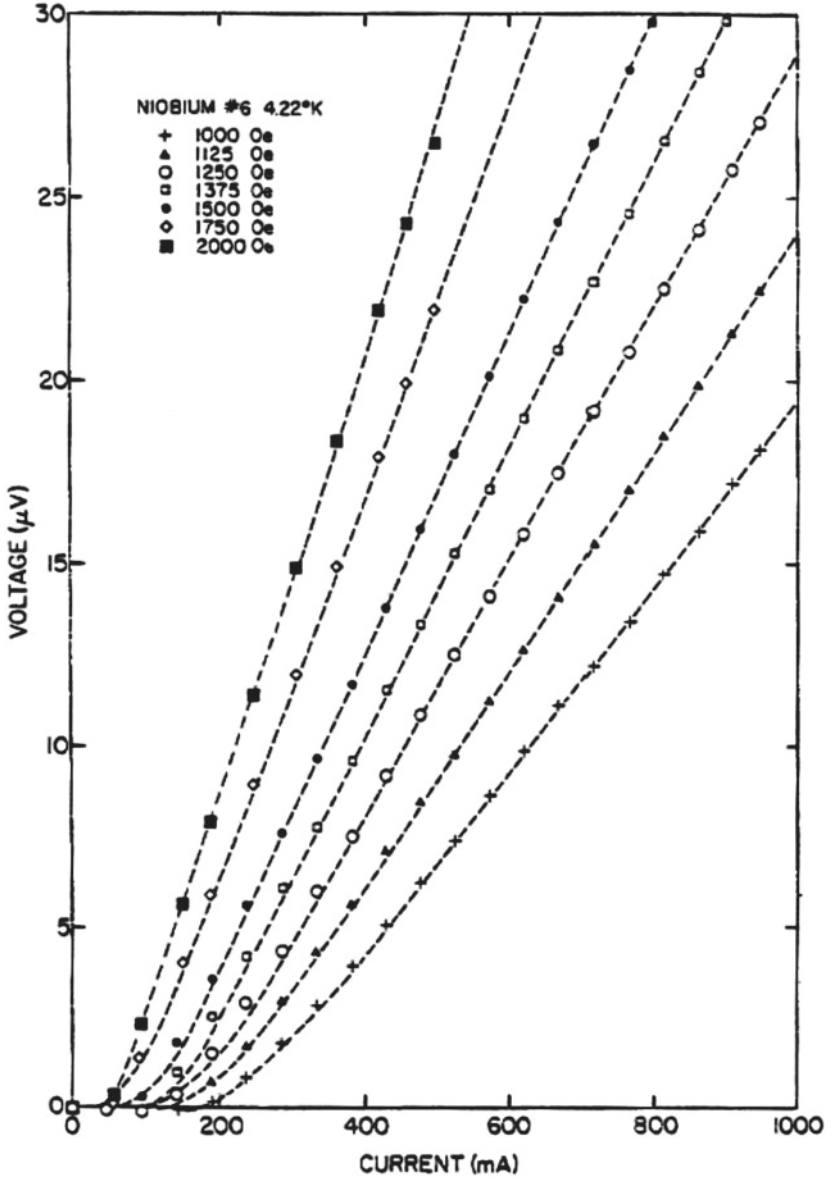

Fig. 8.1 Flux-flow voltage as a function of the electric current in a niobium foil of 18 μm thickness and 4 mm width for various vertically oriented magnetic fields. T = 4.22 K; T_C = 9.2 K

8.1 Thermally Activated Motion of Magnetic Flux Quanta

As already mentioned, the equation of forces (Eq. (8.2)) is an idealized approximation that neglects the effect of pinning forces on the magnetic flux lines. In the following, we want to discuss a special problem from the very complex field of the effect of pinning forces on the magnetic flux line lattice in more detail: the thermally activated movement of the magnetic flux lines.

The basic ideas from the 1960s go back to the abovementioned Philip W. Anderson and Young Kim. We consider a single magnetic flux quantum that is fixed in a potential well by the pinning force. (The potential well represents a local minimum in the spatial course of the Gibbs free energy density.) The depth of the potential well is denoted by U_o. Thermal activation allows the flux quantum to jump out of the potential well, the hopping rate R_j being given by

$$R_j = \nu_o \exp\left(-\frac{U_o}{k_B T}\right) \tag{8.4}$$

Here ν_o denotes a characteristic attempt-frequency, and we assume $U_o \gg k_B T$. In the absence of an external force acting on the flux quantum, the thermally activated hopping process of the flux quantum is the same in all directions, and the resulting flux motion vanishes. However, if an external force acts on the flux

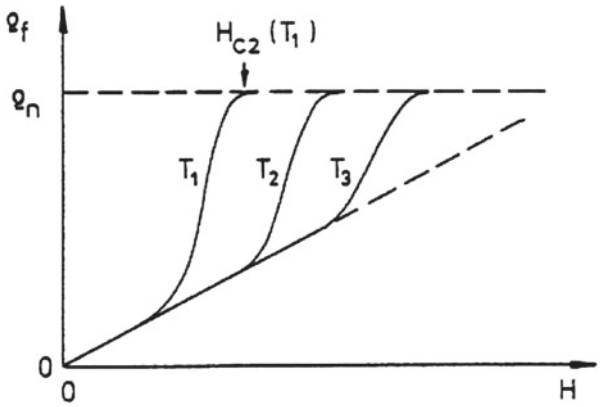

Fig. 8.2 Schematic representation of the specific flux flow resistance ρ_f in a type II superconductor as a function of the magnetic field for different temperatures ($T_1 > T_2 > T_3$). ρ_n denotes the normal resistance

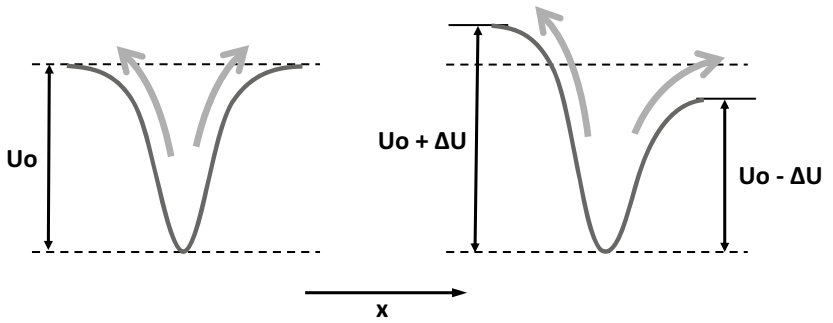

Fig. 8.3 Thermally activated motion of magnetic flux quanta. *Left* Without an external force, the flux jumps do not show a preferred direction. *Right* In the presence of an external force, the flux jumps show a preferred direction

quantum, this spatial symmetry is broken. In the direction of this force, the wall height of the potential well is reduced by ΔU, and in the opposite direction, it is increased by ΔU. In Fig. 8.3, we show a schematic representation. The hopping process now has a preferred direction.

After a short calculation, two important limiting cases are found, where the critical electric current density j_c is decisive, where the energy gain by the Lorentz force exactly compensates the depth of the potential well: $\Delta U = U_o$. In the limit of thermally activated flux flow (TAFF limit), $j \ll j_c$, the following applies:

$$E = 2\rho_c \cdot \exp\left(-\frac{U_o}{k_B T}\right) \cdot \frac{U_o}{k_B T} \cdot j \tag{8.5}$$

and in the limit $j \approx j_c$:

$$E \approx \rho_c \cdot \exp\left[-\frac{U_o}{k_B T}\left(1 - \frac{j}{j_c}\right)\right] \cdot j_c \tag{8.6}$$

In the TAFF limit, we get *Ohm's law* (Eq. (8.5)). However, the resistance E/j is strongly reduced due to the factor $\exp(-U_o/k_B T)$. The limit $j \approx j_c$ of Eq. (8.6) is called *flux creep* with the current-dependent effective energy $U_{eff} = U_o\,(1 - j/j_c)$ of the barrier. This current-dependent exponent in Eq. (8.6) often causes a strong increase of E with increasing j over many orders of magnitude.

The case $j \gg j_c$ is called *flux flow*, for which pinning effects are negligible, just like for a perfectly homogeneous sample. (In the latter case, only the edges of the

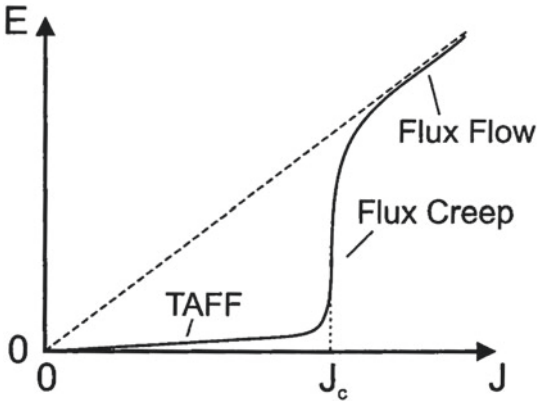

Fig. 8.4 Electric field E as a function of the electric current density J for the different ranges of the physical behavior of the magnetic flux quanta

sample play a role as spatial inhomogeneity). Figure 8.4 shows a summary of the different ranges we have discussed.

9 Cuprate Superconductors

The discovery of so-called *high-temperature superconductors* by Johannes Georg Bednorz and Karl Alexander Müller in 1986 marked the beginning of a new era in the field of superconductivity. The two had found a sudden decrease in electrical resistance by at least three orders of magnitude in compounds of barium (Ba), lanthanum (La), copper (Cu) and oxygen (O) with falling temperature. The drop had started at about 35 K, and it was suspected that this was a new type of superconductivity. However, since superconductivity started at temperatures up to 12 K higher than the record critical temperature of 23.2 K for the compound Nb_3Ge, which had been in existence for 12 years at the time, caution and skepticism were called for.

In the case of Bednorz and Müller, however, the period of skepticism did not last long, as their results were already confirmed at the end of 1986. In 1987, Paul Ching-Wu Chu and colleagues reported a sensational progress: In a modification of the original oxides, in which the larger lanthanum atom was replaced by the smaller yttrium atom, they observed the enormous increase in the critical temperature up to 92 K. The critical temperature of 92 K of this recently discovered new material $YBa_2Cu_3O_7$ (abbreviated YBCO) is even significantly higher than the boiling temperature of 77 K for liquid nitrogen. Now the relatively expensive liquid helium as coolant could be replaced by the much cheaper liquid nitrogen.

An overview of the time course of the discovery of the different superconductors with their critical temperature T_C is shown in Fig. 9.1.

The new class of "cuprate superconductors" (Fig. 9.2) consists of oxides with perovskite structure. They are composed of copper oxide (CuO_2) planes in which the copper and oxygen atoms form a two-dimensional lattice. The crystallographic unit cells of each compound contain a different number of copper oxide planes. A distinction is made between five main families of cuprate superconductors, whose "progenitors" and critical temperatures T_C are listed in Table 9.1.

R. P. Huebener, *History and Theory of Superconductors,* Springer essentials,
https://doi.org/10.1007/978-3-658-32380-6_9

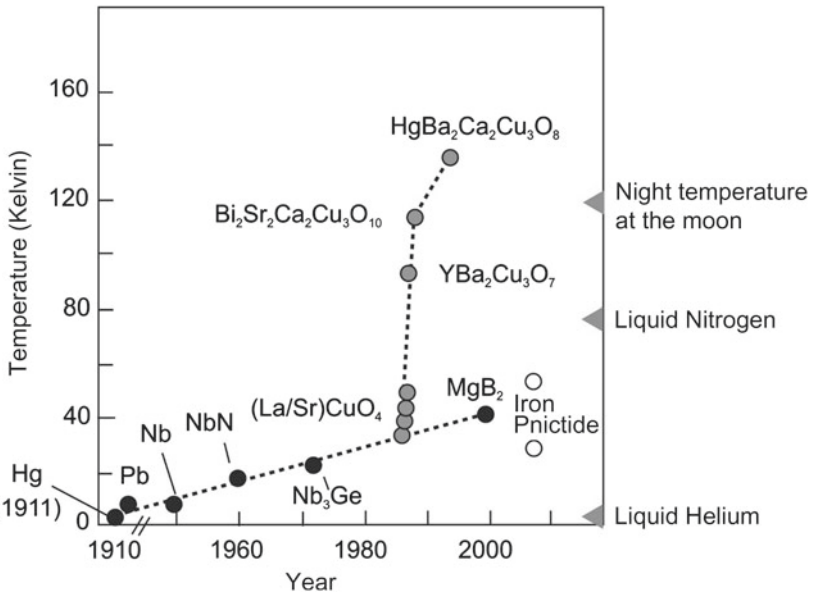

Fig. 9.1 Critical temperature T_C plotted over the year of discovery of various superconductors. The steep curve branch on the right shows some high temperature superconductors. (R. Kleiner)

The copper oxide planes of the cuprates determine the electrical and especially the superconducting properties. Doping with electrical charge carriers plays an important role in this process. In the undoped state, the cuprates are initially electrical insulators. The elementary magnets of the copper atoms in the CuO_2 planes are alternately oriented in opposite directions (antiferromagnetism). Superconductivity only occurs when the electron concentration in the CuO_2 planes is reduced by *doping with holes.* For example, this hole doping is caused by the extraction of oxygen. However, superconductivity only occurs in a relatively narrow concentration range of the doping, so that the oxygen concentration must be carefully controlled during material preparation. Table 9.1 shows the critical temperature values for the case of optimum hole doping. The highest critical temperature value observed so far at normal pressure, $T_C = 133$ K, was found in the compound $HgBa_2Ca_2Cu_3O_{8+x}$. At high pressure, this compound even shows a critical temperature of 164 K.

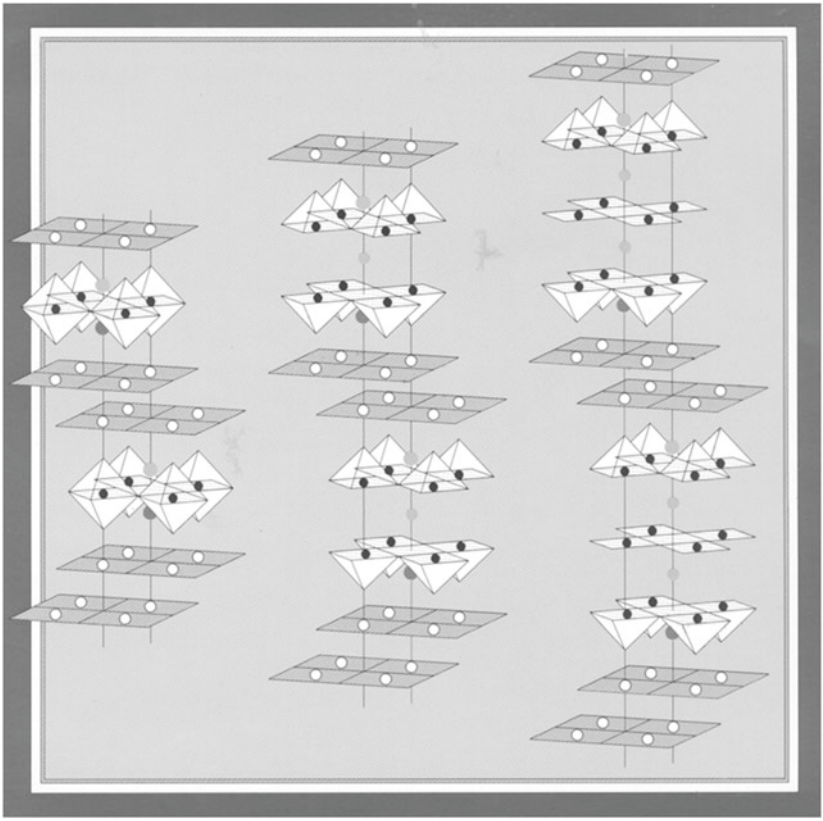

Fig. 9.2 Crystal structure of different cuprate superconductors. At the 6 corners of the light octahedrons or at the 5 corners of the light pyramids, there are oxygen atoms. The centers of the octahedrons or the base of the pyramids are occupied by copper atoms (IBM)

Table 9.1 Critical temperatures of various high-temperature superconductors

Compound	T_C (K)
$La_{2-x}Sr_xCuO_4$	38
$YBa_2Cu_3O_{7-x}$	92
$Bi_2Sr_2CaCu_2O_{8+x}$	110
$Tl_2Ba_2Ca_2Cu_3O_{10+x}$	125
$HgBa_2Ca_2Cu_3O_{8+x}$	133

In contrast to doping with holes, *doping with electrons,* i.e., with negative charges, is necessary for superconductivity in some compounds. However, the concentration range of the doping required for superconductivity is lower in this case and the critical temperature is significantly lower than for compounds doped with holes.

As expected, the layered crystal structure of the cuprate superconductors with its structure of the CuO_2 planes (Fig. 9.2) causes a strong dependence of the electrical and thermal transport properties on the crystal direction. The electrical resistivity in the normal state perpendicular to the CuO_2 planes is up to several orders of magnitude higher than parallel to these planes. In the normal state of the cuprates, the temperature dependence of the electrical resistance, the Hall effect, as well as the Seebeck and Peltier effect, shows a behavior that clearly differs from that of metals.

Soon after the discovery of high-temperature superconductors, it was recognized that the coherence length ξ, which characterizes the spatial rigidity of the superconducting properties, is much smaller in these materials than in classical superconductors. Its size is in the range of the dimensions of the crystallographic unit cell. This leads to a particularly high sensitivity to atomic defects and grain boundaries. Since the coherence length also determines the extent of the core of the magnetic flux lines (see Fig. 5.3), atomic defects and grain boundaries already act as pinning sites for magnetic flux quanta. From the density of the condensation energy of Eq. (2.4), we can see that per unit length of the magnetic flux line, the condensation energy $\left(H_C^2/8\pi\right)\pi\xi^2$ has to be provided for the normal nucleus. This energy can be saved in whole or in part if the core of the flux line passes through a region of the superconductor in which superconductivity is already suppressed by the material inhomogeneity of a pinning center.

The granular structure and spatial inhomogeneity of cuprate superconductors was initially a difficulty that had to be overcome if technical applications of these materials were to be realized. In Fig. 9.3, we show an early example using one of the first prepared thin films of the cuprate superconductor $Y_1Ba_2Cu_3O_7$ with further explanations in the legend.

In the case of cuprate superconductors, the question of whether the formation of Cooper pairs is the central mechanism for superconductivity, as in classical superconductors, could be clarified early on. The positive answer was found from the size of the magnetic flux quantum and the relation between electric voltage and frequency in the Josephson effect, where the double elementary charge of the Cooper pairs always occurred. However, the microscopic pairing mechanism of the cuprates has not yet been clarified.

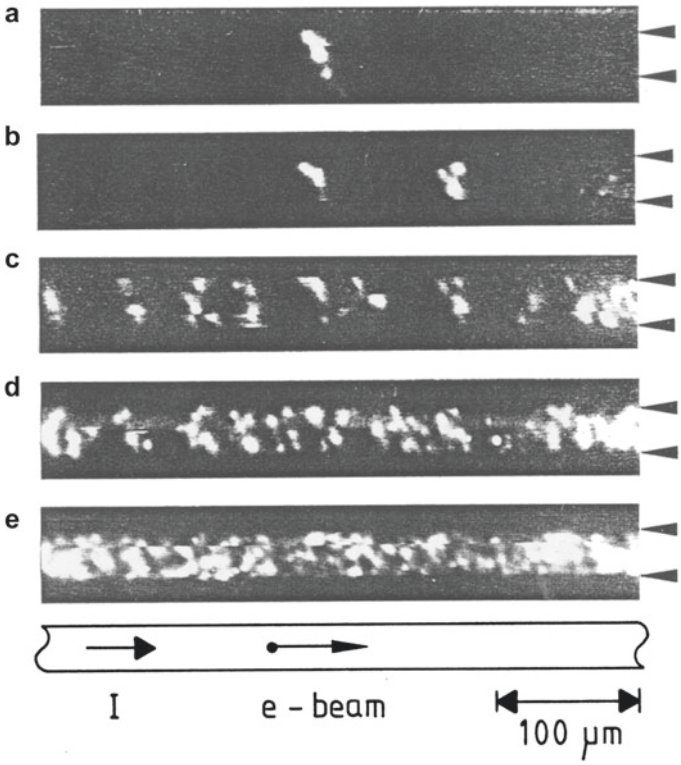

Fig. 9.3 Granular structure of one of the first prepared thin films of the cuprate superconductor $Y_1Ba_2Cu_3O_7$. The layer running horizontally in the figure has a width of 30 μm. The arrowheads on the right mark the upper and lower edges of the layer. Bright spots indicate the locations where electrical resistance occurs in the layer when exposed to electrical current. The dark areas are superconducting. In the series of figures (a) to (e), the electrical current was successively increased from 0.7 mA at (a) to 8.7 mA at (e). The figures show the strong spatial inhomogeneity of the layer with large fluctuations in the local critical electrical current density. The figures were taken using the method of low temperature scanning electron microscopy. The temperature was 53 K

The upper critical magnetic field H_{C2} in cuprate superconductors is up to more than 100–200 times greater than the highest values in classical superconductors. This can be understood using the Ginzburg–Landau theory and the extremely small values of the coherence length.

9.1 Symmetry of the Wave Function

With the reference to the Ginzburg–Landau theory in Chap. 5 and to the BCS theory in Chap. 6, we had presented the macroscopic wave function (Eq. (5.1)) to describe the state of the superconducting electrons. In the case of the cuprate superconductors, we have to discuss especially the symmetry of this wave function. In classical superconductors, the wave function is generally isotropic (s-wave symmetry). In the case of the cuprates, however, the layer structure with the CuO_2 planes must already be taken into account. To illustrate the symmetry of the wave function, a representation in the momentum space is useful. In the two-dimensional **k**-space, which is spanned by k_x and k_y, the amplitude of the wave function is plotted as a function of direction.

In the case of hole-doped high-temperature superconductors, the wave function shows a strong directional dependence, which is determined by the atomic d-orbitals of the copper atoms in the CuO_2 planes. In Fig. 9.4, we show the polar plot of the amplitude of the wave function in two-dimensional **k**-space with the four lobes of the d-orbitals. As a function of the polar angle, we can see the nodes and antinodes as well as the alternating sign. The crystallographic arrangement of the nodes and antinodes is shown for the case of $d_{x^2-y^2}$ symmetry. The isotropic case with s-wave symmetry is also shown for comparison. To identify the directions of the nodes and antinodes, we show in Fig. 9.5 the case of the square CuO_2 lattice in the CuO_2 planes.

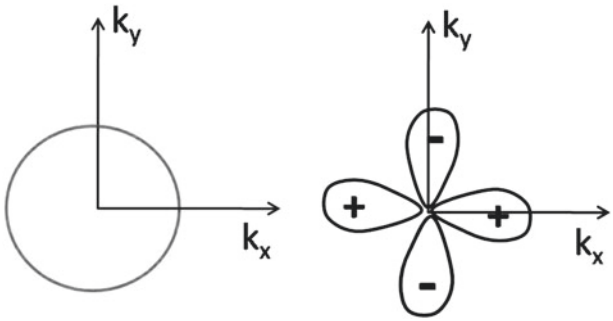

Fig. 9.4 Representation of the wave function with s-wave symmetry (*left*) and with $d_{x^2-y^2}$ symmetry (*right*) in **k**-space (k_x–k_y plane). The latter symmetry dominates in the CuO_2 planes of the cuprate superconductors

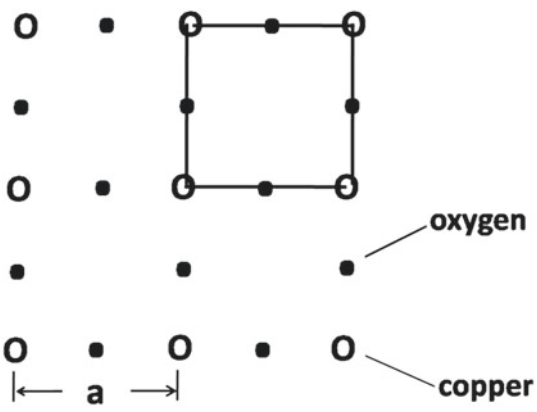

Fig. 9.5 Scheme of the square CuO_2 lattice. The unit cell is marked with the solid line. The lattice constant a is indicated

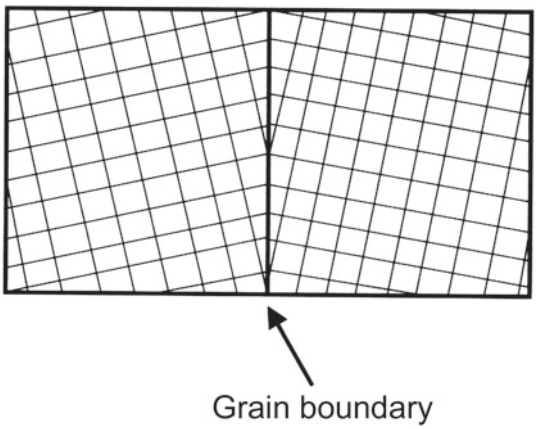

Fig. 9.6 Bicrystal technique for controlled preparation of a single grain boundary in a cuprate superconductor layer. An artificially produced bicrystal is used as substrate, in which two differently oriented monocrystalline parts are separated from each other by an atomically sharp grain boundary. The grain boundary in the substrate is then transferred exactly to the superconductor layer prepared above it. On both sides of the grain boundary, there are monocrystalline superconductor layers with different crystal orientation

The change of sign of the wave function when moving around the coordinate origin in the plane k_x–k_y and the four zero-crossings of the amplitude at the nodes have significant effects on the superconducting properties of materials with d-wave symmetry. The energy gap disappears at the nodes and increases again on both sides.

9.2 Vortex Matter

The layered structure of the cuprate superconductors with the superimposed CuO_2 planes has strong effects on the vortex lattice in the superconducting mixed state. Here we limit ourselves to the case where the magnetic field is oriented perpendicular to the CuO_2 planes. The magnetic flux lines now consist of single small disks, since the superconducting property is limited to the CuO_2 planes. These disks are also called *pancakes*. Due to this decomposition of the individual flux lines, the vortex lattice has numerous new properties. In the literature, this novelty is summarized under the term *vortex matter*. For example, individual disks can now leave their stacked arrangement, which can be regarded as melting and evaporation of the vortex matter.

The new properties of vortex matter are particularly evident in the electrical resistance behavior and electrical losses. As we discussed in Chapter 8, the movement of the magnetic flux lines under the influence of the Lorentz force is the main cause of the electrical losses. This becomes all the more serious when individual parts of the magnetic flux lines can already start moving as small disks. The installation of effective pinning centers is therefore of particular importance. Due to the small coherence length of the cuprates, pinning centers on an atomic length scale, such as missing oxygen atoms in the CuO_2 planes and grain boundaries, are already effective here.

9.3 Grain Boundaries

The granular structure of the oxide cuprate superconductors with their numerous grain boundaries was a great challenge from the very beginning, since superconductivity is generally interrupted within the grain boundaries. The task was therefore to reduce the number of grain boundaries as far as possible. Furthermore, the physical properties of the grain boundaries had to be clarified.

With the help of the already highly developed thin-film technology, it was soon possible to produce monocrystalline thin films of the high-temperature superconductors on suitable substrates. Critical electrical current densities of more than 1 million A/cm^2 could already be achieved at the boiling temperature of liquid nitrogen of 77 K.

The so-called "bicrystal technique" has proven to be very useful for the investigation of grain boundaries. It is based on the following fact. During the epitaxial growth of the high-temperature superconductor layer, the crystal orientation of the monocrystalline substrate is transferred exactly to the superconductor layer above it. If a specially prepared bicrystal is used as a substrate, in which an atomically sharp grain boundary separates two differently oriented crystal regions from each other, then the grain boundary of the substrate is transferred exactly to the superconductor layer prepared above it. In Fig. 9.6, we show the schematic representation of a bicrystal. This bicrystal technique has proved to be very successful in many experiments. In particular, it is very successful in realizing the Josephson effect in high-temperature superconductors. Today, the bicrystal technique is widely used in the fabrication of Superconducting Quantum Interference Devices (SQUIDs) (see Sect. 12.1) based on high-temperature superconductors.

At the end of this section, we will discuss the special case where the bicrystal technique is used to fabricate an arrangement in which two lobes of the superconductor d-wave function meet with different signs. This arrangement is called "π contact". If such a π contact is built into a closed superconducting ring, there is so-called frustration, where the unambiguity of the wave function is destroyed. (A change of sign of the wave function remains after a complete revolution.) In this case, the frustration is cancelled by the spontaneous generation of a half-integer magnetic flux quantum.

In a famous experiment, Chang C. Tsuei and colleagues used this technique to prove the d-wave symmetry of the Cooper pair wave function for the high-temperature superconductors doped with holes. In Fig. 9.7, we show their result. They used a tri-crystal as substrate, in which three monocrystalline regions are arranged in such a way that at one of the three grain boundaries created, a sign change of the wave function occurs between the two sides, thus resulting in a π contact. The frustration is removed by spontaneously forming an exactly half numbered magnetic flux quantum at the common meeting point of the three grain boundaries. The half-integer magnetic flux quantum could be detected with a SQUID scanning microscope.

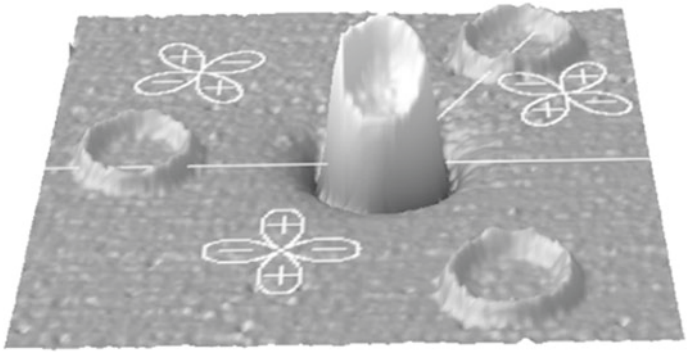

Fig. 9.7 Tri-crystal experiment by Tsuei to prove the d-wave symmetry of the quantum mechanical Cooper pair wave function in the cuprate superconductor $Y_1Ba_2Cu_3O_7$. The substrate is an artificially produced tri-crystal in which three differently oriented monocrystalline crystal parts are separated by atomically sharp grain boundaries. This crystal structure with its grain boundaries is transferred exactly to the superconductor layer prepared above. The grain boundaries are marked by the straight white lines. In the three crystal parts separated by the grain boundaries, the differently oriented d-wave symmetry of the Cooper pair wave function is indicated by the white four-leaf figures. A total of four superconducting rings have been fabricated from the YBaCuO layer at various locations, while the remaining part of the layer has been removed. The orientations of the three crystal parts are chosen in such a way that if d-wave symmetry of the wave function is present, an exactly half-integer magnetic flux quantum is spontaneously generated in the ring around the common meeting point of the three crystal parts, while nothing happens in the remaining three rings. The figure was obtained using a SQUID scanning microscope and shows the half-integer magnetic flux quantum in the middle ring around the common meeting point of the three crystal parts. The other rings remain only weakly indicated (C. C. Tsuei)

9.4 Intrinsic Josephson Contact

The layer structure of the cuprate superconductors with the superconducting CuO_2 layers, which are separated from each other by weakly conducting intermediate layers, suggests that there should be an "intrinsic Josephson effect" here. Reinhold Kleiner and Paul Müller were the first to prove the intrinsic Josephson effect in 1982. Here, several hundred to several thousand Josephson contacts are stacked on top of each other. Initially, Kleiner and Müller used small $Bi_2Sr_2CaCu_2O_8$ (BSCCO) single crystals that were clamped between two contact pins. This allowed an electric current to be passed through the crystal perpendicular to the CuO_2 planes. As soon as an electrical voltage appeared at the contacts above a critical

current level, a high-frequency Josephson alternating current was observed, according to the second Josephson Eq. (7.2), by means of the emitted microwaves. The emitted power of the electromagnetic radiation could be detected because it increases proportionally to the square of the large number of synchronously oscillating Josephson contacts stacked on top of each other in the crystal.

In the meantime, this technique has been further developed. Today, BSCCO towers, so-called "mesas," are used, which are manufactured on a substrate and carry an electrical contact. The principle is shown in Fig. 9.8. The technique is of particular interest as a source of radiation for microwaves in the frequency range 0.5–2 THz, as this frequency range has only been developed to a limited extent so far. Currently, microwave powers of several tens of μW are achieved in the terahertz range for individual mesas. Attempts are being made to increase this power even further by synchronizing networks of several mesas.

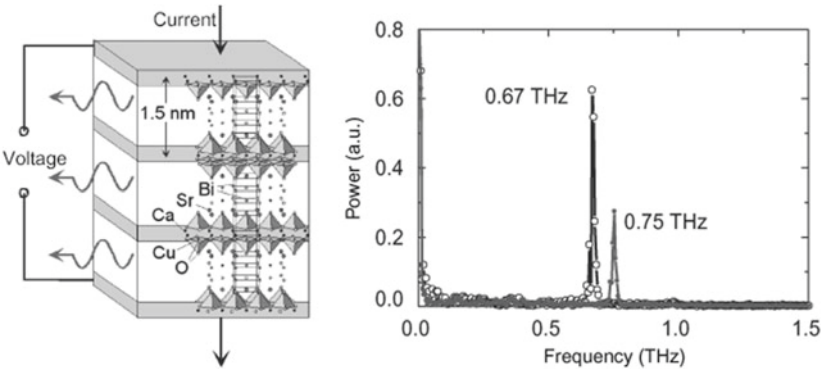

Fig. 9.8 Intrinsic Josephson contact as microwave source. (*Left*) Diagram of a stack of three Josephson contacts of a superconducting $Bi_2Sr_2CaCu_2O_8$ (BSCCO) crystal. The (dark drawn) copper oxide planes run through the base of the CuO pyramids. (*Right*) Emitted microwave spectrum of a BSCCO crystal (R. Kleiner)

MgB_2, Iron Pnictides

10

The search for new superconductors continued even after the discovery of the cuprate superconductors. We will briefly describe the most important developments. In 2001, Jun Akimitsu and colleagues from Tokyo reported the discovery of superconductivity in the compound magnesium diboride (MgB_2) with the critical temperature $T_C = 39$ K. This was very surprising, since the two elements magnesium and boron are not superconducting themselves and the compound had been well known for a long time. The hexagonal crystal structure of MgB_2 shows a layered structure of alternating planes of magnesium and boron atoms. Again, the formation of Cooper pairs due to the electron–phonon interaction is the basis of superconductivity. MgB_2, however, is a case of so-called *two-band superconductivity*, in which charge carriers from two energy bands contribute differently to superconductivity. The wave function of the Cooper pairs shows no clear directional dependence.

The discovery of the iron- and arsenic-containing pnictides in 2008 by Hideo Hosono and colleagues in Japan was another important step. It began with the compound LaOFeAs consisting of lanthanum (La), oxygen (O), iron (Fe) and arsenic (As), which was still doped with fluorine (F). In the compound $LaO_{1-x}F_xFeAs$, the critical temperature $T_C = 26$ K was observed for $x = 0.07$. Also other elements of the light rare earths (Rare Earths, Re) such as praseodymium (Pr), neodymium (Nd) or samarium (Sm) instead of lanthanum resulted in superconducting compounds within the family $ReO_{1-x}F_xFeAs$. Critical temperature values up to the record value $T_C = 56$ K in $Sr_{0.5}Sm_{0.5}FeAsF$ were observed. In their electronic transport properties, the pnictides do not show pronounced anisotropy. The important structural elements are plane layers of iron atoms surrounded by tetrahedrally arranged As- or Se-anions, which play the role of CuO planes in the cuprates (Fig. 10.1). The layers are stacked on top of each other and separated from each other by blocking layers of alkali atoms, elements of the

R. P. Huebener, *History and Theory of Superconductors,* Springer essentials,
https://doi.org/10.1007/978-3-658-32380-6_10

Fig. 10.1 Layers of FeAs (or similarly of FeSe) sandwiched between layers of lanthanum oxide and possibly doped with fluorine

alkaline earths or rare earths and oxygen atoms. For doping, oxygen is partially replaced by fluorine.

Similar to the case of the cuprates 22 years earlier, research on iron pnictides developed explosively worldwide. Similar to the cuprates, the iron pnictides are magnetically ordered in the undoped state. Unlike the cuprates, however, they are electrically conducting. They are an antiferromagnetic semimetal. It seems that in this case, superconductivity and magnetism are related. In Fig. 10.2, we show an overview of the different iron pnictides discovered until 2015. The different families are identified by the names 11, 111, 122, 1111, etc. More than 50 iron pnictides have been found by 2010. The pairing mechanism is still unclear. However, there is much evidence to suggest magnetic spin fluctuations as the basis for the formation of Cooper pairs.

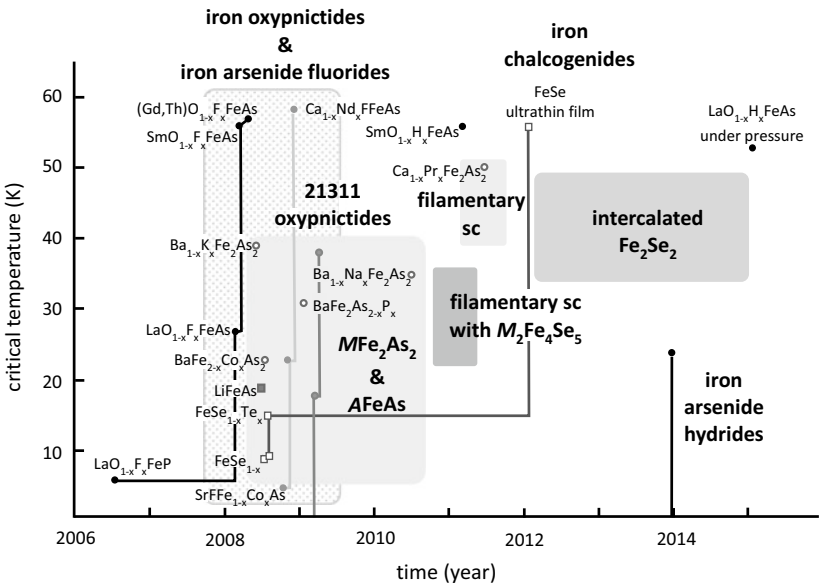

Fig. 10.2 Critical temperature T_C of different iron pnictide superconductors plotted against time of discovery. (Silvia Haindl)

Superconductivity in Interfaces and Monolayers

11

In 2015, an announcement made headlines that superconductivity with a critical temperature above 100 K was observed in FeSe monolayers. The discovery came from China (which, after the end of the Cultural Revolution in 1971, experienced a huge boom, which also extended to the natural sciences). Indications of *superconductivity in FeSe monolayers* had already been given by another Chinese group in 2012. The monolayers were prepared on specially processed $SrTiO_3$ substrates by molecular beam epitaxy (MBE). The thin layers were particularly sensitive and had to be stored in a vacuum or protected from destruction by a cover layer.

Due to the great progress in the field of thin film technology, research into superconductivity in interfaces and monolayers has developed rapidly in recent years. MBE, pulsed laser deposition and sputtering are the most important techniques for the preparation of new materials. Scanning tunneling microscopy (STM) and angle-resolved photoemission spectroscopy (ARPES) are indispensable analytical methods for the investigation of electronic properties.

Before electrical resistance measurements on the FeSe/$SrTiO_3$ monolayers had found the onset of superconductivity at 109 K, there were already indications of a superconducting state through tunnel experiments. These showed that the energy gap in the FeSe monolayers is about ten times larger than in FeSe crystals and that the critical temperature should therefore be correspondingly higher. In crystalline form, FeSe is a superconductor with a critical temperature of 8 K. Apparently, the electron–phonon (electron–boson) coupling between the electrons in the interfaces is significantly increased. Furthermore, mechanical tensions can play a role in the epitaxial films. The FeSe monolayers show a pronounced two-dimensional geometry and are therefore easier to treat theoretically due to the absence of a k_z component of the wave vector (which plays a role in the other Fe-based superconductors). In the two dimensions, the energy gap is isotropic and does not show any zeros (nodes). At a temperature of 3 K, a critical electrical current

R. P. Huebener, *History and Theory of Superconductors,* Springer essentials,
https://doi.org/10.1007/978-3-658-32380-6_11

density of $1.3 \cdot 10^7$ A/cm^2 was measured (in high vacuum) if the monolayer did not have a protective covering layer. With a protective coating, this critical current density was reduced to about 10^6 A/cm^2. Even with a thickness of the FeSe layer of two unit cells and above, superconductivity disappears.

The chemical and structural similarity of many oxides allows the combination of materials with different electronic properties. The system $LaAlO_3/SrTiO_3$ with its interface between two band insulators provided first indications of *superconductivity in interfaces.* Electric conductivity was discovered in 2004 and superconductivity at the interface in 2007. The Cooper pairs apparently exist in the conductive interface, but the reason for the pairing is to be found in the nonconducting neighboring material. This is reminiscent of similar ideas published long before by V. L. Ginzburg (1964), D. Allender, J. Bray and J. Bardeen (1973) and W. Little and H. Gutfreund (1971). In the crystalline state, $LaAlO_3$ and $SrTiO_3$ are electrical insulators with a remarkable energy gap between the valence and conduction bands of 5.6 and 3.2 eV, respectively. The electrically conducting interface is formed when an epitaxial film of $LaAlO_3$ with a thickness of more than three unit cells is deposited on a $SrTiO_3$ single crystal. The crystal structure of $LaAlO_3$ ($SrTiO_3$) consists of successive layers of LaO and AlO_2 (SrO and TiO_2). While the SrO and TiO_2 layers are charge-neutral, the LaO and AlO_2 layers each carry a positive or negative charge. In this way, an electrical potential difference is created between the interface and the LaO surface. To compensate this potential difference, various mechanisms of charge transfer to the $SrTiO_3$ surface have been proposed, whereby an electrically conducting electron fluid is generated there. The local confinement of the electrons in a potential well (quantum confinement) must also be taken into account.

To study superconductivity at the $LaAlO_3/SrTiO_3$ interface, it is useful to modify the charge carrier doping of the two-dimensional electron liquid by means of a gate electrode on the back side of the $SrTiO_3$ substrate and the field effect. Depending on the doping of the interface, the transition to superconductivity shows a dome-like pattern with a maximum value of T_C of about 300 mK. With the help of the field effect, superconductivity can be reversibly switched on and off at low temperatures.

A similar result can be seen in the semiconducting state: After doping, $SrTiO_3$ is also superconducting. The critical temperature also shows a dome-like curve as a function of doping with a maximum value of about 300 mK.

Similar to $LaAlO_3/SrTiO_3$, superconductivity was also found at the interface of $LaTiO_3$ and $SrTiO_3$.

Materials behave differently in two dimensions than in three. This leads to new physical effects, which are being studied with increasing intensity. The field

of superconductivity in interfaces and monolayers is only just beginning and promises to remain interesting.

Technical Applications

12

12.1 Microelectronics

The applications of superconductivity in microelectronics are essentially based on two facts: magnetic flux quantization and the Josephson effect. In both cases, a macroscopic quantum effect and the description of the state of the Cooper pairs with a quantum mechanical wave function play the central role. A characteristic example is the SQUID (abbreviated from Superconducting Quantum Interference Device). The principle is shown in Fig. 12.1, where two parallel Josephson contacts are built into a closed superconducting loop. Due to magnetic flux quantization, the magnetic flux of an external magnetic field through the loop can only assume values of integer multiples of the magnetic flux quantum. This condition is realized by spontaneously generating a circulating supercurrent in the loop in such a way that its magnetic flux together with the external magnetic flux yields exactly one integer multiple of a flux quantum. (We have already shown a similar case in Fig. 5.2.)

This leads to an exactly periodic modulation of the shielding current in the loop depending on the external magnetic field. The circulating electrical shielding current now flows in addition to the external current, so that the electrical voltage drop along the loop arrangement is also periodically modulated. The voltage measurement still allows the resolution of a small fraction of a modulation period, resulting in a high sensitivity for magnetic field measurement. Today, SQUIDs are manufactured using thin film technology and integrated circuit technology.

Their high sensitivity as sensors for magnetic fields makes SQUIDs interesting for many applications. In medical diagnostics, new fields of application have developed that involve the magnetic fields generated by the electrical currents during cardiac activity and in the brain. This has led to the development of the new fields

R. P. Huebener, *History and Theory of Superconductors,* Springer essentials,
https://doi.org/10.1007/978-3-658-32380-6_12

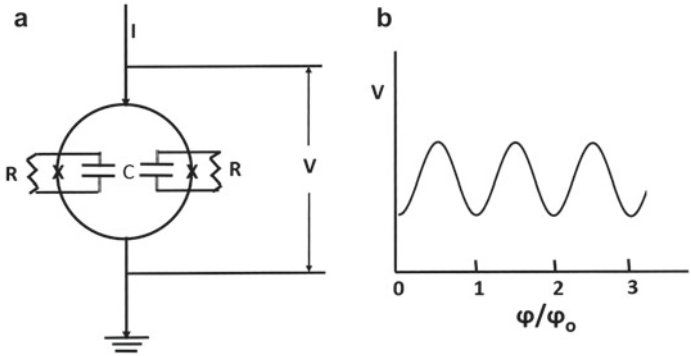

Fig. 12.1 **a** Equivalent circuit diagram of the SQUID. The crosses (X) in the current loop indicate the Josephson contacts, which each contain a shunt resistor (R) and a shunt capacitance (C). **b** Voltage modulation at constant impressed current as a function of the magnetic flux φ in the current loop in units of the flux quantum φ_o

of magnetocardiography and magnetoencephalography. In brain research today, devices with up to 275 SQUID channels are used. The channels with the individual sensors are arranged three-dimensionally around the head of the test person or patient. In Fig. 12.2, we show an example. In SQUID scanning microscopes, especially miniaturized SQUIDs are used. Their high magnetic field sensitivity combined with a spatial resolution of only a few μm allows the imaging of individual magnetic flux quanta in superconductors. An application of a SQUID scanning microscope is shown in Fig. 9.7 of Sect. 9.3. Further applications for SQUIDs can be found in nondestructive materials testing.

At present, small spin systems in nanoparticles are attracting particular attention. The latest development of these SQUID instruments is the production of ultra-small devices on sharp tips on the nano-scale (nano-SQUID-on-tip). By depositing superconducting lead or niobium on the tip of hollow quartz tubes, SQUID loops with an effective diameter of only 160 nm or even less than 100 nm can be achieved. An estimation shows that the signal of a single electron spin located 10 nm below a SQUID-on-tip loop can still be resolved with a spatial accuracy of about 20 nm.

Today, the Josephson effect has numerous applications in so-called *Josephson electronics*. The second Josephson Eq. (7.2) states that an electrical voltage drop at a Josephson contact is always associated with a high-frequency oscillation of the supercurrent between both electrodes of the contact. Here, a voltage

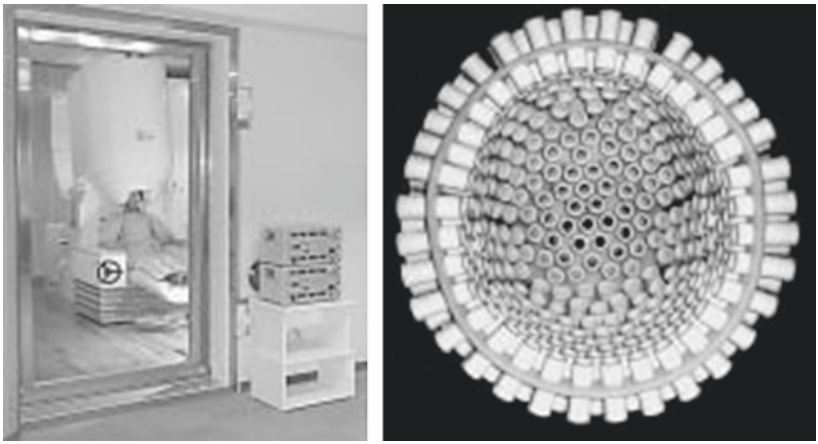

Fig. 12.2 Magnetoencephalography. *Left*: Test subject with the helmet put over his head with the SQUID magnetic field sensors in a magnetically shielded room. *Right*: Interior view of a helmet with 151 SQUID sensors. (Photos: MEG International Services Ltd.)

of 10^{-3} V corresponds to an oscillation frequency of 483.6 GHz. If, on the other hand, a current-carrying Josephson contact is irradiated with a high-frequency electromagnetic wave, for example with a microwave, pronounced electrical voltage plateaus occur at the contact. The second Josephson equation determines the value of the voltage plateau by the frequency of the irradiated electromagnetic wave. Since frequencies can be measured very accurately, this quantum relationship between frequency and electrical voltage has been used since January 1, 1990 for the legal definition of the unit of electrical voltage by the state calibration offices. On the basis of this Josephson voltage standard, a voltage of 1 V corresponds to the frequency 483,597.9 GHz. In this way, the Josephson effect is part of the famous *quantum triangle* of current, voltage and resistance for the definition of electrical units of measurement.

In the case of high-temperature superconductors, the relatively high values of the critical temperature compared with those of classical superconductors in particular have given a great boost to the search for their technical applications. The possibility of using superconductivity already when cooled down to 77 K with liquid nitrogen is particularly attractive. In Sect. 9.3, we mentioned the fabrication of Josephson contacts and SQUIDs on bicrystal substrates in thin films of high temperature superconductors. This method is widely used today. High-frequency filters made of high-temperature superconducting layers are interesting because

they have a greater frequency sharpness of the high-frequency channels so that significantly more channels can be accommodated within the available frequency band. For example, more than 10,000 base stations for mobile telephone traffic are already operated with this technology worldwide. Cooling down to about 70 K is done by so-called cryocoolers, which have been developed in recent years for reliable cooling and which can run maintenance-free for long periods of time.

12.2 Power Engineering

The applications of superconductivity in power engineering, for example, for magnet coils or cables, only became possible when new superconductor materials with higher values of the critical electric current density and the upper critical magnetic field H_{C2} were discovered in the 1960s. The focus was then on the compounds NbTi with $T_C = 9.6$ K and Nb_3Sn with $T_C = 18$ K. At that time, thin layers of the compound Nb_3Ge reached the record value of the critical temperature of classical superconductors with $T_C = 23.2$ K. For industrial production, special drawing and extrusion processes as well as optimized annealing treatments and cold-working were quickly developed. The so-called "multifilamentary wires," which consist of many thin filaments of the superconductor material within a copper matrix, became famous. This technique guarantees certain stability in case of overload and at the same time provides sufficient pinning centers for anchoring the magnetic flux quanta in the superconductor material.

Superconducting magnetic coils are an important product today, especially for research. In Fig. 12.3, we show two examples. Large beam guiding magnets for particle accelerators and the associated particle detector systems are indispensable today. The "Large Hadron Collider" (LHC) at the European Nuclear Research Center (CERN) in Geneva has been in operation for several years as the world's largest particle accelerator based on superconductivity.

Another large-scale application of superconductivity is found in magnetically levitated trains. Recently, especially the Japanese JR-Maglev project has made good progress. In 2015, tests showed that a speed of over 600 km/h was achieved. Superconducting coils are mounted in the train, which generate magnetic fields above 5 T. Electrically well-conducting current loops are built into the track bed, in which strong eddy currents are generated when the train passes by. According to Lenz's rule, the magnetic field of the eddy currents causes a repulsive force on the field of the coils and thus the levitating force. Since this repulsion is only sufficiently strong above a certain minimum speed, the train must first run on wheels, which are retracted when this speed is reached.

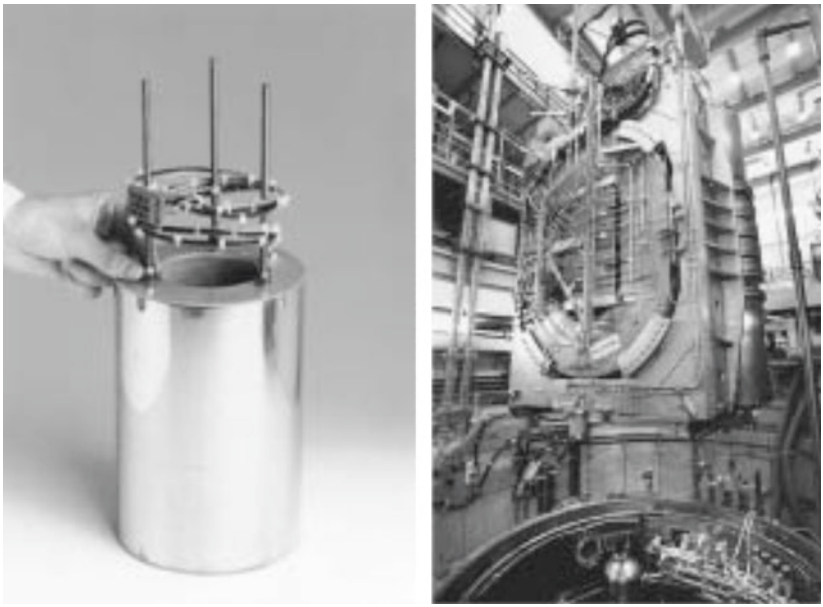

Fig. 12.3 Superconducting magnet coils. **(Left)** Commercially available coil for research purposes. The coil is wound from niobium-titanium (NbTi) wire and can generate a magnetic field up to 9 T (about 1 million times the Earth's magnetic field). (Oxford.) **(Right)** Superconducting model coil with its test setup for a toroidal magnetic field when entering the cryogenic container of an experimental facility at the Karlsruhe Research Center (Forschungszentrum Karlsruhe). The experimental facility is used to develop the technology for magnetic plasma confinement during nuclear fusion. The external dimensions of the oval model coil are 2.55 m × 3.60 m × 0.58 m. During operation, an electric current of 80,000 amperes flows through the coil. The entire test assembly weighs 107 tons and shall be cooled to 4.5 K. The cryogenic container has a usable inside diameter of 4.3 m and a usable height of 6.6 m (Forschungszentrum Karlsruhe)

An important market for superconductivity technology has developed over the last 30 years due to the superconductive magnets used in magnetic resonance imaging. This was helped by the fact that at the beginning of the 1980s, the health authorities allowed magnetic resonance imaging for medical diagnostics. The annual turnover of the industry in this field today amounts to 2–3 billion EUR.

Superconducting energy transmission cables with classical superconductors have also been investigated since the 1970s in various pilot projects. Cooling with

liquid helium was envisaged. Superconducting energy transmission cables are of particular interest where the usual overhead lines are not possible in conurbations.

Superconducting magnetic energy storage devices based on magnetic coils operated with direct current are an interesting technology for storing electrical energy. They can be useful for bridging short interruptions in the electrical energy supply. Finally, superconducting coils are indispensable in nuclear fusion to generate the high magnetic fields required for plasma confinement. The largest superconducting magnet systems are currently being developed for this long-term energy supply option.

In the field of high-current applications, intensive work is being done on the development of magnetic coils made of *high-temperature superconductors.* Furthermore, superconducting systems for electrical current limitation in power engineering are in a promising stage of development. These systems are intended to enable rapid interruption of the electrical current if overload threatens to cause damage to the electrical lines. A particularly interesting new development is currently (2015) in generators made of high-temperature superconductors for electrical power generation by wind energy. Their planned use would halve the weight of the generator located at the top of the mast compared to the previous equipment or double the power for the same weight.

What You Learned From This *essential*

- How young and unknown scientists often make key discoveries
- That the close cooperation between experimentalists and theorists can be necessary for important advances
- That the Physikalisch-Technische Reichsanstalt (PTR) in Berlin founded in 1887 by Werner Siemens and Hermann von Helmholtz became an extremely successful and important research institution
- How the engineering development of the technology for the preparation of epitaxial thin films lead to important advances in science and technology
- How the preparation of new materials and hetero-structures lead to unexpected advances in the field of superconductivity

R. P. Huebener, *History and Theory of Superconductors,* Springer essentials,
https://doi.org/10.1007/978-3-658-32380-6

Literatur

Bennemann, K.H., Ketterson, J.B. (Hrsg.): The physics of superconductors, Bd. 1 und 2. Springer, Berlin (2003)

Blatter, G., Feigel'man, M.V., Geshkenbein, V.B., Larkin, A.I., Vinokur, V.M.: Vortices in high-temperature superconductors. Rev. Mod. Phys. **66**, 1125 (1994)

Buckel, W., Kleiner, R.: Supraleitung – Grundlagen und Anwendungen, 7th edn. Wiley-VCH, Weinheim (2013)

CCAS Document: Superconductivity – present and future applications

De Gennes, P.G.: Superconductivity of metals and alloys. W. A. Benjamin, New York (1966)

Gariglio, S., Gabay, M., Mannhart, J., Triscone, J.-M.: Interface superconductivity. Physica C **514**, 189 (2015)

Goodman, B.B.: Type II superconductors. Rep. Prog. Phys. **29**(2), 445 (1966)

Huebener, R.P.: Magnetic flux structures in superconductors, 2nd edn. Springer, Berlin (2001)

Ketterson, J.B., Song, S.N.: Superconductivity. Cambridge University Press, Cambridge (1999)

Komarek, P.: Hochstromanwendung der Supraleitung. Teubner, Stuttgart (1995)

Lynton, E.A.: Superconductivity. Methuen & Co, London (1962)

Parks, R.D. (Hrsg.): Superconductivity, Bd. 1 und 2. Marcel Dekker, New York (1969)

Poole, C., Farach, H.A., Creswick, R.J.: Superconductivity. Academic, New York (1995)

Qi, X.-L., Zhang, S.-C.: Topological insulators and superconductors. Rev. Mod. Phys. **83**, 1057 (2011)

Rickayzen, R.: Theory of superconductivity. Wiley, New York (1965)

Tinkham, M.: Introduction to superconductivity, 2nd edn. McGraw-Hill, New York (1996)

Waldram, J.R.: Superconductivity of metals and cuprates. Institute of Physics Publishing, Bristol (1996)

Historical development

Dahl, P.F.: Superconductivity – its historical roots and development from mercury to the ceramic oxides. American Institute of Physics, New York (1992)

Cooper, L.N., Feldman, D. (eds.): BCS – 50 Years. World Scientific, Hackensack (2011)

Rogalla, H., Kes, P.H. (eds.): 100 years of superconductivity. CRC Press, Boca Raton (2012)

R. P. Huebener, *History and Theory of Superconductors,* Springer essentials,
https://doi.org/10.1007/978-3-658-32380-6